

A Theoretical Study of Top-Mass Measurements at the LHC Using NLO+PS Generators of Increasing Accuracy

Silvia Ferrario Ravasio,^a Tomáš Ježo,^b Paolo Nason,^c Carlo Oleari^a

^a*Università di Milano-Bicocca and INFN, Sezione di Milano-Bicocca, Piazza della Scienza 3, 20126 Milano, Italy*

^b*Physics Institute, Universität Zürich, Zürich, Switzerland*

^c*CERN, CH-1211 Geneve 23, Switzerland, and INFN, Sezione di Milano-Bicocca, Piazza della Scienza 3, 20126 Milano, Italy*

E-mail: silvia.ferrario@mib.infn.it, tomas.jezo@physik.uzh.ch,
paolo.nason@mib.infn.it, carlo.oleari@mib.infn.it

ABSTRACT: In this paper we study the theoretical uncertainties in the determination of the top-quark mass using next-to-leading-order (NLO) generators interfaced to parton showers (PS) that have different levels of accuracy. Specifically we consider three generators: one that implements NLO corrections in the production dynamics, one that includes also NLO corrections in top decay in the narrow width approximation, and one that implements NLO corrections for both production and decay including finite-width and interference effects. Our aim is to provide an assessment of the uncertainties of purely theoretical origin, we thus consider simplified top-mass related observables that are broadly related to those effectively used by experiments, eventually modelling experimental resolution effects with simple smearing procedures. Examining these observables with generators of increasing accuracy allows us to assess the theoretical errors due to the use of the less accurate generators. Furthermore, we estimate theoretical uncertainties associated with the variation of scales and with the choice of parton distribution functions. In order to give an indicative assessment of the uncertainties due to the shower and to the modelling of non-perturbative effects, we interface our NLO+PS generators to both `Pythia8.2` and `Herwig7.1`, with various settings, and compare the results.

KEYWORDS: QCD, Hadronic Colliders, Monte Carlo simulations, NLO calculations.

Contents

1	Introduction	1
2	NLO+PS generators	5
2.1	Interface to shower generators	6
2.1.1	Generic method	6
2.1.2	Standalone implementations in <code>Pythia8.2</code>	7
2.1.3	Standalone implementations in <code>Herwig7.1</code>	8
3	Phenomenological analysis setup	9
3.1	Physics objects	9
3.2	Generated sample	10
4	Anatomy of the reconstructed top mass distribution at NLO+PS	10
4.1	Les Houches event level comparison of the generators	11
4.2	Shower effects	13
4.3	Hadronization and underlying events	13
5	Methodology	15
6	Reconstructed top mass distribution m_{Wb_j}	16
6.1	Comparison among the different NLO+PS generators	17
6.1.1	Renormalization- and factorization-scale dependence	20
6.1.2	PDF set dependence	21
6.1.3	Strong-coupling dependence	21
6.1.4	Matching uncertainties	22
6.1.5	Summary of scale, PDF and α_s variations	22
6.1.6	Radius dependence	24
6.2	Comparison with <code>Herwig7.1</code>	24
6.2.1	Alternative matching prescriptions in <code>Herwig7.1</code>	27
7	The energy of the b jet	29
7.1	Comparison among different NLO+PS generators	30
7.2	Comparison with <code>Herwig7.1</code>	32
8	Leptonic observables	34
8.1	Comparison among NLO+PS generators	34
9	Summary	38
10	Conclusions	43
A	The treatment of remnants	44

B Fitting procedure	46
C PowhegHooks.h	46
D Truncated showers	47

1 Introduction

The abundant production of top pairs at the Large Hadron Collider (LHC) provides an opportunity for detailed studies of top-quark properties, for tests of the Standard Model (SM), and for measurements of fundamental parameters such as the top-quark mass. With the Higgs boson mass now known with high precision, the W -boson and top-quark masses have become strongly correlated, and an accurate determination of both would lead to a SM test of unprecedented precision [1, 2]. The present value of the indirect top-mass determination from electroweak precision data (176.7 ± 2.1 GeV, see [1]) is in slight tension, at the 1.6σ level, with the direct measurements. The latest combination of the Tevatron and the LHC results [3] yields 173.34 ± 0.76 GeV, but more recent results favour even smaller values, close to 172.5 GeV, see [4–7]. Recent reviews of top-mass measurements by the ATLAS and CMS collaborations can be found in Refs. [8] and [9].

It has been shown that in Standard Model as is (i.e. assuming no new physics effects up to the Planck scale), the vacuum is stable if the top mass, m_t , is below 171 GeV (i.e. very close to its present value), metastable up to 176 GeV, and unstable above this value [10–12]. The current value is safely below the instability region. However, it should not be forgotten that the absence of new physics up to the Planck scale is a very strong assumption. The only conclusion we can draw from these results is that there is no indication of new physics below the Planck scale coming from the requirement of vacuum stability. On the other hand, the fact that the Higgs boson quartic coupling almost vanishes at the Planck scale may have some deep meaning that we are now unable to unveil.

Besides the issues related to electroweak tests and the stability of the vacuum, the question on how precisely we can measure the top mass at hadron colliders also has its own significance, related to our understanding of QCD and collider physics. In view of the large abundance of top-pair production at the LHC, it is likely that precise measurements will be performed with very different methods, and that comparing them will give us confidence in our ability to handle hadron-collider physics problems.

Top-mass measurements are generally performed by fitting m_t -dependent kinematic distributions to Monte Carlo predictions. The most precise ones, generally called *direct measurements*, rely upon the full or partial reconstruction of the system of the top-decay products. The CMS and ATLAS measurements of Refs. [5] and [4], yielding the value $m_t = 172.44 \pm 0.13$ (stat) ± 0.47 (syst) GeV and 172.84 ± 0.34 (stat) ± 0.61 (syst) GeV respectively, fall into this broad category.

The top mass cannot be defined in terms of the mass distribution of the system of its decay products: since the top quark is a coloured object, no final-state particle system

can be unambiguously associated with it. On the other hand, the top mass is certainly related to the mass distribution of the system of certain objects arising from top decay, i.e. hard leptons, neutrinos and hard, b -flavoured hadronic jets. The mass distribution of this system can be computed and measured, and the top mass enters this computation as a parameter. By extracting its value from a fit to the measured distributions, we are unavoidably affected by theoretical errors that must be carefully assessed. In particular, these errors will depend upon the accuracy of the modelling of these distributions.

The absence of a “particle-level truth” for the top-decay products has led to speculations that the top mass cannot be extracted reliably in the direct measurements. The extracted mass is unavoidably a parameter in the theoretical calculation or in the Monte Carlo generator that is used to compute the relevant distributions. It has thus been argued that, because of this, and since shower Monte Carlo (SMC) models are accurate at leading order (LO) only, the extracted mass cannot be identified with a theoretically well-defined mass, such as the pole mass or the $\overline{\text{MS}}$ mass (that differ among each other only at the NLO level and beyond).

In the present work, we use NLO-accurate generators, so that the previously mentioned objection does not actually apply. Moreover, it can be argued that, in the narrow width approximation and at the perturbative level, the mass implemented in Monte Carlo generators corresponds to the pole mass [13] even if we do not use NLO-accurate generators.

It was also argued in Ref. [14] that the Monte Carlo mass parameter differs from the top pole mass by an amount of the order of a typical hadronic scale, that was there quantified to be near 1 GeV. It is further argued that this difference is, in fact, intrinsic in the uncertainty with which the pole mass can even be defined, because of the presence of a renormalon in the relation of the pole to the $\overline{\text{MS}}$ mass [15, 16].

Recent studies [17, 18] have shown that the renormalon ambiguity in the top-mass definition is not as large as previously anticipated, being in fact well below the current experimental error. The fact remains, however, that non-perturbative corrections to top-mass observables (not necessarily related to the mass renormalon) are present, can affect a top-mass determination, and are likely to be parametrically of the order of a typical hadronic scale. We believe, however, that this does not justify the introduction of a “Monte Carlo mass” concept, since it is unlikely that non-perturbative effects, affecting top-mass observables, can be parametrized as a universal shift of the top-mass parameter. The real question to answer is whether these non-perturbative effects are of the order of 100 MeV, 1 GeV, or more. While a top-mass determination from threshold production at e^+e^- collider would be free of such uncertainties [19, 20],¹ at hadron colliders, non-perturbative effects of this order are likely to affect, to some extent, most top-mass observables that have been proposed so far.²

The theoretical problems raised upon the top-quark mass measurement issues have induced several theorists to study and propose alternative methods. In Ref. [22], observables relevant to $t\bar{t}$ + jet kinematics are presented. The authors of Ref. [23] presented a method

¹ This is also the case for a top-mass determination based upon the spectrum of $\gamma\gamma$ production near the $t\bar{t}$ threshold [21], that however is likely to be statistically limited, even at the high luminosity LHC.

²For a recent discussion of all these issues see Ref. [13].

based upon the charged-lepton energy spectrum, that is not sensitive to the top production kinematics, but only upon the top decay, arguing that, since this has been computed at NNLO accuracy [24, 25], a very accurate measurement may be achieved. Some authors have advocated the use of boosted top jets (see Ref. [26] and references therein). In Ref. [27], the authors make use of the b -jet energy peak, that is claimed to have reduced sensitivity to production dynamics. In Ref. [28], the use of lowest Mellin moments of lepton kinematic distributions is discussed. In the leptonic channel, it is possible to use distributions based on the “stransverse” mass variable [29], which generalizes the concept of transverse mass for a system with two identical decay branches [30, 31].

Some of these methods have in fact been exploited [29, 32–35] to yield alternative determinations of m_t . It turns out, however, that the direct methods yield smaller errors at the moment, and it is likely that alternative methods, when reaching the same precision level, will face similar theoretical problems.

In this work, we exploit the availability of the new POWHEG BOX [36–38] generators for top-pair production, i.e. the $t\bar{t}dec$ [39] and $b\bar{b}4\ell$ [40] ones, in order to perform a theoretical study of uncertainties in the top-mass determination. In particular, we are in a position to assess whether NLO corrections in top decay, that are implemented in both the $t\bar{t}dec$ and $b\bar{b}4\ell$ generators, and finite width effects, non-resonant contributions and interference of radiation generated in production and decay, that are implemented in $b\bar{b}4\ell$, can lead to sizable corrections to the extracted value of the top mass. Since the $h\nu q$ generator [41], that implements NLO corrections only in production, is widely used by the experimental collaborations in top-mass analyses, we are particularly interested in comparing it with the new generators, and in assessing to what extent it is compatible with them.³ We will consider variations in the scales, parton distribution functions (PDFs) and jet radius parameter to better assess the level of compatibility of the different generators.

We are particularly interested into effects that can be important in the top-mass determination performed in direct measurements. Thus, the main focus of our work is upon the mass of a reconstructed top, that we define as a system comprising a hard lepton, a hard neutrino and a hard b jet. We will assume that we have access to the particle level truth, i.e. that we can also access the flavour of the b jet, and the neutrino momentum and flavour. We are first of all interested in understanding to what extent the mass peak in the reconstructed top depends upon the chosen NLO+PS generator. This would be evidence that the new features introduced in the most recent generators are mandatory for an accurate mass extraction.

We will also consider the inclusion of detector effects in the form of a smearing function applied to our results. Although this procedure is quite crude, it gives a rough indication of whether the overall description of the process, also outside of the reconstructed resonance peak, affects the measurement.

³The $h\nu q$ and $t\bar{t}dec$ generators can be found under the `User-Processes-V2` directory of the POWHEG BOX V2 repository in the `h\nu q` and `ttb_NLO_dec` directories, respectively. The $b\bar{b}4\ell$ generator can be found under the `User-Processes-RES/b.bbar_4l` directory of the POWHEG BOX RES code. Detailed instructions are found in the powhegbox.mib.infn.it.

Besides studying different NLO+PS generators, we have also attempted to give a first assessment of ambiguities associated with shower and non-perturbative effects, by interfacing our NLO+PS generators to two shower Monte Carlo programs: `Pythia8.2` [42] and `Herwig7.1` [43, 44]. We are aware that much more work in this direction should be performed, by also considering variations of parameters and options within the same parton shower generator.⁴

We have also considered two alternative proposals for top-mass measurements: the position of the peak in the b -jet energy [27] and the leptonic observables of Ref. [28]. The first proposal is an example of a hadronic observable that should be relatively insensitive to the production mechanism, but may be strongly affected by NLO corrections in decay. The second proposal is an example of observables that, in principle, depend also upon the production mechanism, so that we may expect more sensitivity to scale variation and PDFs. Furthermore, these observables are built only from the lepton momenta. Thus, it is interesting to study their sensitivity to hadronization, in order to see whether there is any ground to the generic assumption that leptonic observables should have a reduced dependence upon these effects.

The impact of NLO corrections in decays and finite-width effects were also considered in Ref. [48] for a number of top-mass related observables, and in Ref. [49] for the method relying upon the $t\bar{t}j$ final state. Here we are more interested in observables related to direct measurements, that are not considered there. Furthermore, we focus our studies upon the differences with respect to the widely-used $h\nu q$ generator.

The paper is organized as follows. In Sec. 2 we briefly review the features of the $h\nu q$, $t\bar{t}dec$ and $b\bar{b}4\ell$ generators. We also discuss the interfaces to the parton-shower programs `Pythia8.2` and `Herwig7.1`.

In Sec. 3, we detail the setup employed for the phenomenological studies presented in the subsequent sections.

In Sec. 4, we perform a generic study of the differences of our generators focusing upon the mass distribution of the $W b$ -jet system. The aim of this section is to show how this distribution is affected by the different components of the generators, by examining results at the Born level, after the inclusion of NLO corrections, after the parton shower, and at the hadron level.

In Sec. 5 we describe how we relate the computed value of our observables to the corresponding value of the top mass that would be extracted in a measurement.

In Sec. 6 we consider as our top-mass sensitive observable the peak position in the mass distribution of the reconstructed top, defined as the mass of the system comprising the hardest lepton and neutrino, and the jet with the hardest b -flavoured hadron, all of them with the appropriate flavour to match a t or a \bar{t} . We study its dependence upon the NLO+PS generator being used, the scale choices, the PDFs, the value of α_s and the

⁴An interesting example of work along this direction can be found in Refs. [45] and [46], where the impact of the colour reconnection model on top-mass measurement is analyzed. In Ref. [47], a study is performed to determine whether the use of jet-grooming techniques in top-mass measurement can reduce the Monte Carlo tune dependence.

jet radius parameter. Furthermore, we present and compare results obtained with the two shower Monte Carlo generators `Pythia8.2` and `Herwig7.1`.

We repeat these studies for the peak of the b -jet energy spectrum [27] in Sec. 7, and for the leptonic observables [28] in Sec. 8.

In Sec. 9 we summarize our results, and in Sec. 10 we present our conclusions. In the appendices we give some technical details.

2 NLO+PS generators

In this section we summarize the features of the `POWHEG BOX` generators used in the present work, i.e. the $h\nu q$, the $t\bar{t}dec$ and the $b\bar{b}4\ell$ generators.

The $h\nu q$ program [41] was the first top-pair production generator implemented in `POWHEG`. It uses on-shell matrix elements for NLO production of $t\bar{t}$ pairs. Off-shell effects and top decays, including spin correlations, are introduced in an approximate way, according to the method presented in Ref. [50]. Radiation in decays is fully handled by the parton-shower generators. The ones that we consider, `Pythia8.2` and `Herwig7.1`, implement internally matrix-element corrections for top decays, with `Herwig7.1` also optionally including a `POWHEG`-style hardest-radiation generation. In these cases, their accuracy in the description of top decays is, for our purposes, equivalent to the NLO level.

The $t\bar{t}dec$ code [39] implements full spin correlations and NLO corrections in production and decay in the narrow-width approximation. Off-shell effects are implemented via a reweighting method, such that the LO cross section includes them exactly. As such, it contains also contributions of associated top-quark and W -boson production at LO. It does not include, however, interference of radiation generated in production and decay.

In $t\bar{t}dec$ the `POWHEG` method has been adapted to deal with radiation in resonance decays. Radiation is generated according to the `POWHEG` Sudakov form factor both for the production and for all resonance decays that involve coloured partons. This feature also offers the opportunity to modify the standard `POWHEG` single-radiation approach. Rather than picking the hardest radiation from one of all possible origins (i.e. production and resonance decays), the `POWHEG BOX` can generate simultaneously the hardest radiation in production and in each resonance decays. The LH events generated in this way can thus carry more radiated partons, one for production and one for each resonance. Multiple-radiation events have to be completed by a shower Monte Carlo program, that has to generate radiation from each origin without exceeding the hardness of the corresponding `POWHEG` one, thus requiring an interface that goes beyond the simple Les Houches standard [51].

A general procedure for dealing with decaying resonances that can radiate by strong interactions has been introduced and implemented in a fully general and automatic way in a new version of the `POWHEG BOX` code, the `POWHEG BOX RES` [52]. This framework allows for the treatment of off-shell effects, non-resonant subprocesses including full interference, and for the treatment of interference of radiation generated in production and resonance decay.⁵ In Ref. [40] an automated interface of the `POWHEG BOX RES` code to the `OpenLoops` [54]

⁵A related approach within the `MC@NLO` framework has been presented in Ref. [53].

matrix-element generator has been developed and used to build the $b\bar{b}4\ell$ generator, that implements the process $pp \rightarrow b\bar{b}e^+\nu_e\mu^-\bar{\nu}_\mu$, including all QCD NLO corrections in the 4-flavour scheme, i.e. accounting for finite b -mass effects. So, double-top, single-top and non-resonant⁶ diagrams are all included with full spin-correlation effects, radiation in production and decays, and their interference.

As for the $t\bar{t}dec$ generator, $b\bar{b}4\ell$ can generate LH events including simultaneous radiation from the production process and from the top and anti-top decaying resonances. It thus requires a non-standard interface to parton-shower Monte Carlo programs, as for the case of the $t\bar{t}dec$ generator.

2.1 Interface to shower generators

According to the **POWHEG** method, the PS program must complete the event only with radiation softer than **POWHEG** generated one. In the standard Les Houches Interface for User Processes (LHIUP) [51], each generated event has a hardness parameter associated with it, called **scalup**. This parameter is set in **POWHEG** to the relative transverse momentum of the generated radiation and each emission attached by the parton shower must have p_T smaller than its value. The LHIUP treats all emissions on an equal footing, and has no provision for handling radiation from decaying resonances. This drives a standard PS to allow showering to start from scales of the order of the resonance mass.

2.1.1 Generic method

References [39] and [40] introduce a generic method for interfacing **POWHEG** processes that include radiation in decaying resonances with PS generators. According to this method, shower radiation from the resonance is left unrestricted, and a veto is applied *a posteriori*: if any radiation in the decaying resonance shower is harder than the **POWHEG** generated one, the event is discarded, and the same LH event is showered again. We also stress that the standard PS implementations conventionally preserve the mass of the resonance, as long as the resonance decay products, including eventually the radiation in decay, have the resonance as mother particle in the LH event record.

The hardness of the radiation associated with the decaying top ($t \rightarrow W b g$) in **POWHEG** is given by

$$t = 2 \frac{E_g}{E_b} p_g \cdot p_b = 2 E_g^2 (1 - \beta_b \cos \theta_{bg}), \quad (2.1)$$

where $p_{g/b}$ and $E_{g/b}$ are the four momentum and energy of the gluon and of the bottom quark, β_b is the velocity of the bottom quark and θ_{bg} is the angle between the bottom and gluon momenta, all evaluated in the top rest frame. This hardness definition is internally used to define the corresponding Sudakov form factor. The same should be also used to limit the transverse momentum generated by the PS in the resonance decay.

The practical implementation of the veto procedure depends on whether we are using a dipole, as in **Pythia8.2**, or an angular-ordered shower, as in **Herwig7.1**. If we are using a dipole (p_T -ordered) shower, it is sufficient to check the first shower-generated emission from

⁶By non-resonant we mean processes that do not contain an intermediate top quark, e.g. $pp \rightarrow b\bar{b}Z \rightarrow b\bar{b}W^+W^- \rightarrow b\bar{b}e^+\nu_e\mu^-\bar{\nu}_\mu$.

the bottom quark and (if present at the LH level) from the gluon arising in top decay. The hardness t_b of the shower-generated emission from the bottom is evaluated using eq. (2.1), while the one from the gluon is taken to be

$$t_g = 2 E_1^2 E_2^2 \frac{(1 - \cos \theta_{12})}{(E_1 + E_2)^2}, \quad (2.2)$$

where $E_{1,2}$ are the energies of the two gluons arising from the splitting, and θ_{12} is the angle between them. Both t_g and t_b are computed in the top frame. If they are smaller than t , the event is accepted, otherwise it is showered again.

In the case of angular-ordered showers, as in `Herwig7.1`, it is not enough to examine the first emission, because the hardest radiation may take place later. As shown in Ref. [36], in the leading logarithmic approximation, the hardest emission in an angular-ordered shower can be always found by following either the quark line in a $q \rightarrow qg$ splitting, or the most energetic line in a $g \rightarrow gg$ splitting. Thus, when inspecting the sequence of splittings, in order to find the hardest radiation, if the parton that generates the shower is a fermion (in our case, the b/\bar{b} quark), we simply follow the fermionic line; in case of a gluon splitting, we follow the most energetic gluon. We go on until either the shower ends, or we reach a $g \rightarrow q\bar{q}$ splitting. Since this last process is not soft-singular, configurations with the hardest emission arising after it are suppressed.

2.1.2 Standalone implementations in Pythia8.2

The `Pythia8.2` generator provides facilities for implementing the above-described method to veto internally radiation in resonance decays. We prepared two implementations, each based on a different facility, and now we describe them in turn.

1. At every radiation generated by `Pythia8.2`, a function is called internally using `UserHooks` facility. The function inspects the radiation kinematics. If the radiation comes from top decays, it computes its transverse momentum, according to eqs. (2.1) and (2.2). If the transverse momentum is larger than the one of the radiation generated by `POWHEG` in the resonance decay, the emission is vetoed, and `Pythia8.2` tries to generate another splitting. The process is repeated until an acceptable splitting is generated. This behaviour is achieved by implementing the method

```
UserHooks::doVetoFSREmission,
```

whose description can be found in the `Pythia8.2` manual [55]. It is activated by setting the `Pythia8.2` flag

```
POWHEG:bb41:FSREmission:veto = on.
```

2. `UserHooks` facility also allows us to set the initial scale of final-state shower evolution (for the shower arising from the decaying resonances) equal to the transverse momentum of the top radiation in decay. This is achieved using the method

`UserHooks::scaleResonance,`

and is activated by setting the `Pythia8.2` flag

`POWHEG:bb41:ScaleResonance:veto = on`

This method has the disadvantage of relying upon the assumption that the hardness definition used by `Pythia8.2` is compatible with the `POWHEG` one.

Both methods are implemented in the file

`PowhegHooksBB4L.h`

in the $b\bar{b}4\ell$ subprocess directory.

We have chosen implementation 1 as our default, and compared it with the other implementations in order to validate it and estimate matching uncertainties.

2.1.3 Standalone implementations in `Herwig7.1`

Also in the case of `Herwig7.1` we have prepared two implementations that use the MC internal facilities to perform the veto:

1. After the whole time-like shower has been developed, but before hadronization has been carried out, the showers from the b and from the `POWHEG` radiated gluon in top decay are examined. In the case of the b , the quark line is followed, and the transverse momentum of the radiation is computed (in the top frame) according to eq. (2.1). In the case of the gluon, the hardest line is followed, and the transverse momentum of the radiation is computed according to eq. (2.2). If a radiation is found with transverse momentum harder than the `POWHEG` generated one, the full event is reshowered, starting from the same LH event. The corresponding method is called

`FullShowerVeto::vetoShower,`

and we have implemented it in the files

`bb41FullShowerVeto.h, bb41FullShowerVeto.cc.`

2. We veto each radiation in resonance decay if its transverse momentum is harder than the `POWHEG` generated one. In this case, `Herwig7.1` tries again to generate radiation starting from the (angular ordering) hardness parameter of the vetoed one. As in `Pythia8.2` second method, we have to rely in this case upon the `Herwig7.1` definition of the radiation transverse momentum. The corresponding method is called

`ShowerVeto::vetoTimeLike`

and we implemented it in the files

`bb41ShowerVeto.h, bb41ShowerVeto.cc.`

We will adopt the implementation 2 as our `Herwig7.1` default, and compare with the other ones in order to validate it, and also in order to get an indication of the size of matching uncertainties.

3 Phenomenological analysis setup

We simulate the process $pp \rightarrow b\bar{b}e^+\nu_e\mu^-\bar{\nu}_\mu$, which is available in all three generators. It is dominated by top-pair production, with a smaller contribution of Wt topologies. For the observables we consider, the decay of one of the two top quarks is mostly irrelevant, so that our result will also hold for semileptonic decays.

In the $h\nu q$ and $t\bar{t}dec$ generators we renormalize the top mass in the pole-mass scheme, while in the $b\bar{b}4\ell$ one we adopt the complex mass scheme [40], with the complex mass defined as $\sqrt{m_t^2 - i m_t \Gamma_t}$.

We perform our simulations for a center-of-mass energy of $\sqrt{s} = 8$ TeV. We have used the MSTW2008nlo68c1 PDF set [56] and we have chosen as central renormalization and factorization scale (μ_R and μ_F) the quantity μ , defined, following Ref. [40], as the geometric average of the transverse masses of the top and anti-top

$$\mu = \sqrt[4]{(E_t^2 - p_{z,t}^2)(E_{\bar{t}}^2 - p_{z,\bar{t}}^2)}, \quad (3.1)$$

where the top and anti-top energies $E_{t/\bar{t}}$ and longitudinal momenta $p_{z,t/\bar{t}}$ are evaluated at the underlying-Born level.

In the $b\bar{b}4\ell$ case, there is a tiny component of the cross section given by the topology

$$pp \rightarrow Zg \rightarrow (W^+ \rightarrow e^+\nu_e)(W^- \rightarrow \mu^-\bar{\nu}_\mu)(g \rightarrow b\bar{b}). \quad (3.2)$$

In this case we define μ as

$$\mu = \frac{\sqrt{p_Z^2}}{2}, \quad (3.3)$$

where $p_Z = p_{\mu^-} + p_{\bar{\nu}_\mu} + p_{e^+} + p_{\nu_e}$. This case is however very rare and unlikely to have any significance.

The parameter `hdamp` controls the separation of remnants (see Appendix A) in the production of $t\bar{t}$ pairs with large transverse momentum. We set it to the value of the top mass.

3.1 Physics objects

In our simulations we make the B hadrons stable, in order to simplify the definitions of b jets. Jets are reconstructed using the Fastjet [57] implementation of the anti- k_T algorithm [58] with $R = 0.5$. We denote as B (\bar{B}) the hardest (i.e. largest p_T) b (\bar{b}) flavoured hadron. The b (\bar{b}) jet is the jet that contains the hardest B (\bar{B}).⁷ It will be indicated as j_B ($j_{\bar{B}}$). We discard events where the b jet and \bar{b} jet coincide. The hardest e^+ (μ^-) and the hardest ν_e ($\bar{\nu}_\mu$) are paired to reconstruct the W^+ (W^-). The reconstructed top (anti-top) quark is identified with the corresponding W^+j_B ($W^-j_{\bar{B}}$) pair. In the following we will refer to the mass of this system as m_{Wb_j} .

We require the two b jets to have

$$p_T > 30 \text{ GeV}, \quad |\eta| < 2.5. \quad (3.4)$$

⁷Note that this notation is the opposite of what is commonly adopted for B mesons, where B refers to the meson containing the \bar{b} quark.

	Generated samples									
	m_t [GeV]						$\alpha_s(m_Z)$			
	172.5		169.5		175.5		0.115		0.121	
	# events	time	# events	time	# events	time	# events	time	# events	time
hvq	12M	10 h	3M	2.5 h	3M	2.5 h	12M	9 h	12M	9 h
$t\bar{t}dec$	12M	46 d	3M	11.5 d	3M	11.5 d	12M	25 d	12M	25 d
$b\bar{b}4\ell$	20M	4600 d	1.7M	390 d	1.7M	390 d	3M	64 d	3M	64 d

Table 1. Number of events and total CPU time of the generated samples. The samples used for the α_s variations were obtained in a relatively smaller time, since in this case only the central weight was computed. This leads to a difference that can be sizable, depending upon the complexity of the virtual corrections.

These cuts suppress the single-top topologies. The hardest e^+ and the hardest μ^- must satisfy

$$p_T > 20 \text{ GeV}, \quad |\eta| < 2.4. \quad (3.5)$$

3.2 Generated sample

For each generator under study, we have produced three samples of events, each sample computed with a top mass of 169.5, 172.5 and 175.5 GeV, respectively, with the corresponding decay width computed at NLO. Using the reweighting feature of the **POWHEG BOX**, we have computed the event weights obtained by varying the parton distribution functions and the renormalization and factorization scales, for a total of 12 weights (see Secs. 6.1.1 and 6.1.2 for more details).

In the reweighting procedure, only the inclusive **POWHEG** cross section is recomputed. The Sudakov form factor is not recomputed, so that the radiated partons retain the same kinematics. For this reason, the change of the renormalization and factorization scales do not affect the emission of radiation. Thus, in order to investigate the sensitivity of the result on the intensity of radiation, where we are particularly concerned with emissions from the final-state b quarks, we have also generated samples with the **NPDF30_nlo_as115** and **NNPDF30_nlo_as121**, with $\alpha_s(m_Z) = 0.115$ and $\alpha_s(m_Z) = 0.121$ respectively, for each generator, for the central value of the top mass, i.e. 172.5 GeV. The number of events for each generated sample, together with an indicative computational time, are reported in Tab. 1.

4 Anatomy of the reconstructed top mass distribution at NLO+PS

In this section we investigate the impact of individual ingredients in a typical NLO+PS calculation on the kinematic distribution of the reconstructed top mass m_{Wb_j} . On the perturbative side, we examine the impact of the different level of accuracy in the treatment of top production and decay provided by the three generators we are considering, and the impact of parton-shower effects. On the non-perturbative side, we illustrate the effect of including hadronization and underlying event in the simulation.

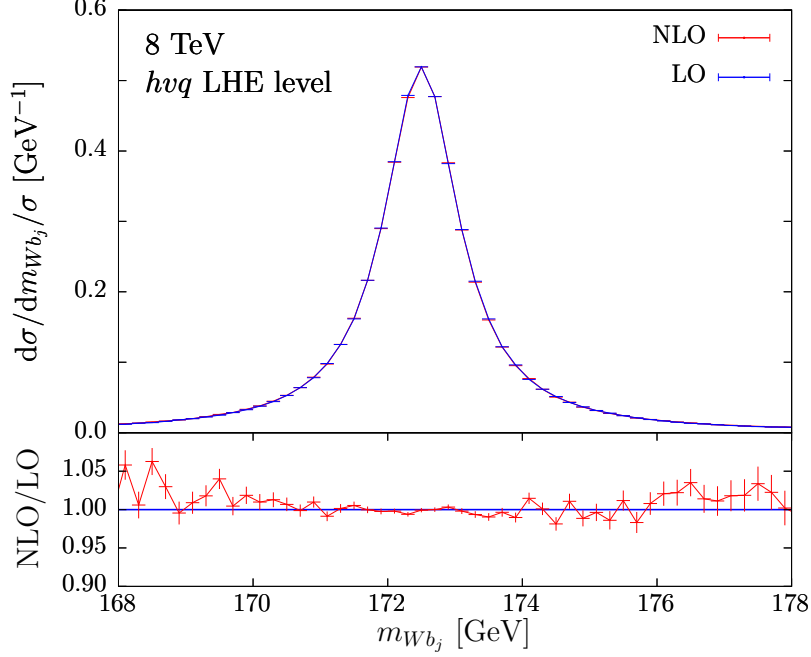


Figure 1. $d\sigma/dm_{Wb_j}$ distribution at LO (blue) and at NLO (red) obtained with the *h_vq* generator, normalized to 1 in the displayed range. In the bottom panel the ratio with the LO prediction is shown.

4.1 Les Houches event level comparison of the generators

We begin by comparing the three generators at the Les Houches event (LHE) level. In Figs. 1 and 2 we compare m_{Wb_j} , normalized to 1 in the displayed range, at LO and NLO accuracy using the *h_vq* and the *b \bar{b} 4 ℓ* generators respectively. The *h_vq* generator includes NLO corrections only in the production process. Thus the m_{Wb_j} distributions at LO and NLO are very similar. On the other hand, in the case of the *b \bar{b} 4 ℓ* generator (Fig. 2), we observe large differences below the peak region. These differences are easily interpreted as due to radiation outside the *b*-jet cone in the top-decay process.

The *t \bar{t} dec* generator allows us to specify whether NLO accuracy is required both in production and decay (default behaviour), or just in production (by using the `nlowhich 1` option). In Fig. 3 we compare the two options. We see that our previous observation is confirmed: the impact of NLO corrections in production leads to a roughly constant *K*-factor, while the radiation from top decay affects the shape of the distribution below the peak region.

A remaining important difference between the *h_vq* and the other two generators has to do with the way the distribution of the top virtuality is modeled. The *b \bar{b} 4 ℓ* and *t \bar{t} dec* generators are guaranteed to yield the correct virtuality distribution at the NLO and LO level, respectively. This not the case for the *h_vq* generator, where the resonance structure is recovered by a reweighting procedure that does not guarantee LO accuracy. This is illustrated in Fig. 4, where we see that a non-negligible (although not dramatic) difference in shape is present also at the LO level between the *h_vq* and the other two generators.

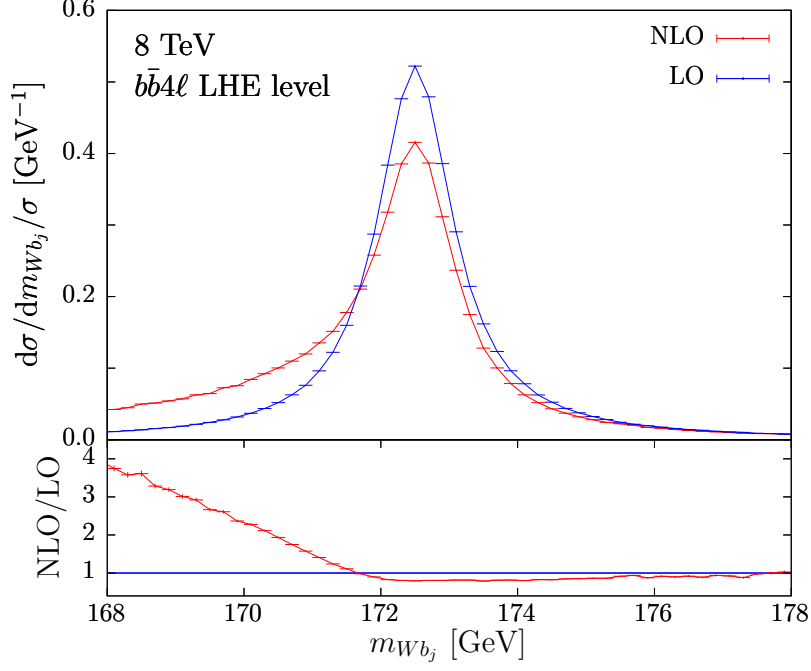


Figure 2. $d\sigma/dm_{Wb_j}$ distribution at LO (blue) and at NLO (red) obtained with the $b\bar{b}4\ell$ generator, normalized to 1 in the displayed range. In the bottom panel the ratio with the LO prediction is shown.

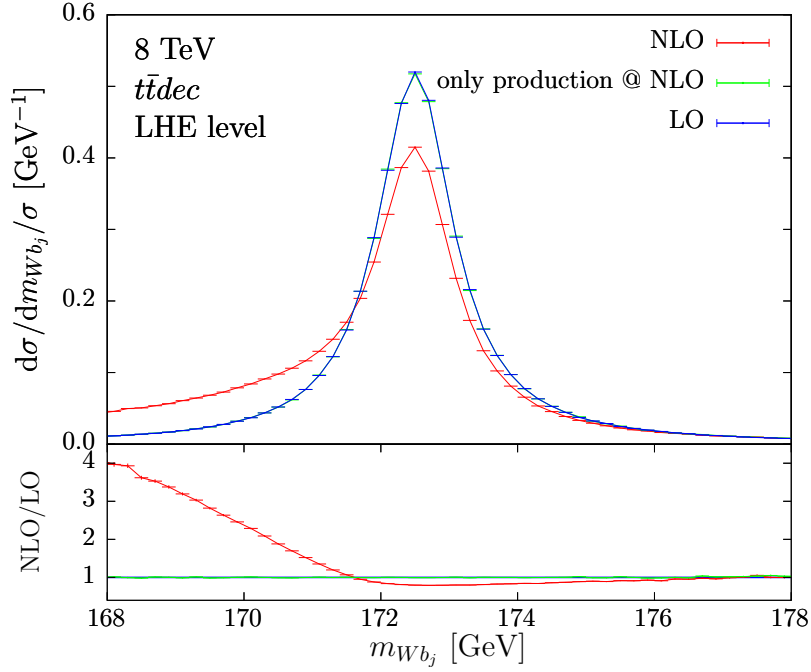


Figure 3. $d\sigma/dm_{Wb_j}$ distribution with NLO accuracy in production and decay (red), only in production (green) and with LO accuracy (blue) obtained with the $t\bar{t}dec$ generator, normalized to 1 in the displayed range. In the bottom panel the ratio with the LO prediction is shown.

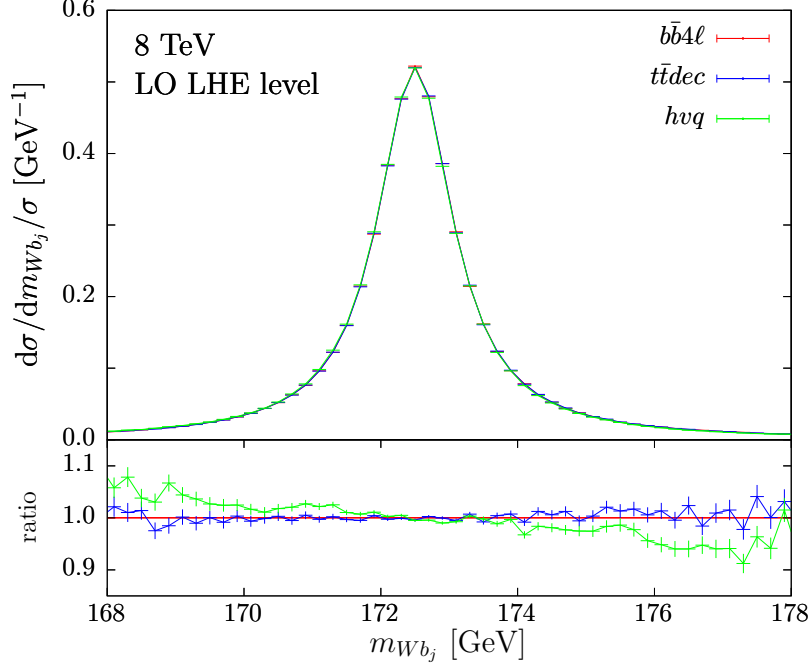


Figure 4. $d\sigma/dm_{Wb_j}$ distribution at LO obtained with $bb4l$ (red), $t\bar{t}dec$ (blue) and hvq (green), normalized to 1 in the displayed range. In the bottom panel the ratio with the $bb4l$ prediction is shown.

4.2 Shower effects

We now examine how the shower, i.e. the radiation beyond the hardest one, affects our distributions. First of all, we anticipate an important effect in hvq , since in this case radiation in decay is fully generated by the shower. We thus expect a raise of the low mass tail in the m_{Wb_j} distribution, comparable in size to the one observed in the $bb4l$ and $t\bar{t}dec$ generators at the LHE level. Conversely, in the $bb4l$ and $t\bar{t}dec$ cases, we expect smaller shower corrections, since the hardest radiation in decay is already included at the LHE level. This is illustrated in Fig. 5, where we clearly see that in the hvq case there is an important increase of the cross section below the peak. On the other hand, in the $bb4l$ case this increase is minor or even absent, depending upon which shower program is used. In both cases, we see an enhancement in the region above the peak. This is attributed to shower radiation that is captured by the b -jet cone. We observe that, after shower, the hvq result becomes qualitatively very similar to the $bb4l$ one, as shown in Fig. 6.

The inclusion of the shower in $t\bar{t}dec$ leads to effects similar to those observed in $bb4l$.

4.3 Hadronization and underlying events

In Fig. 7 we show the effect of hadronization and multi-parton interactions (MPI), as modeled by `Pythia8.2` and `Herwig7.1`, when interfaced to the hvq generator. We can see the large effect of the hadronization on the final distribution. This effect is also considerably different between `Pythia8.2` and `Herwig7.1`. There are two main features that emerge in these plots. First of all, as expected, the MPI raise the tail of the distributions above the

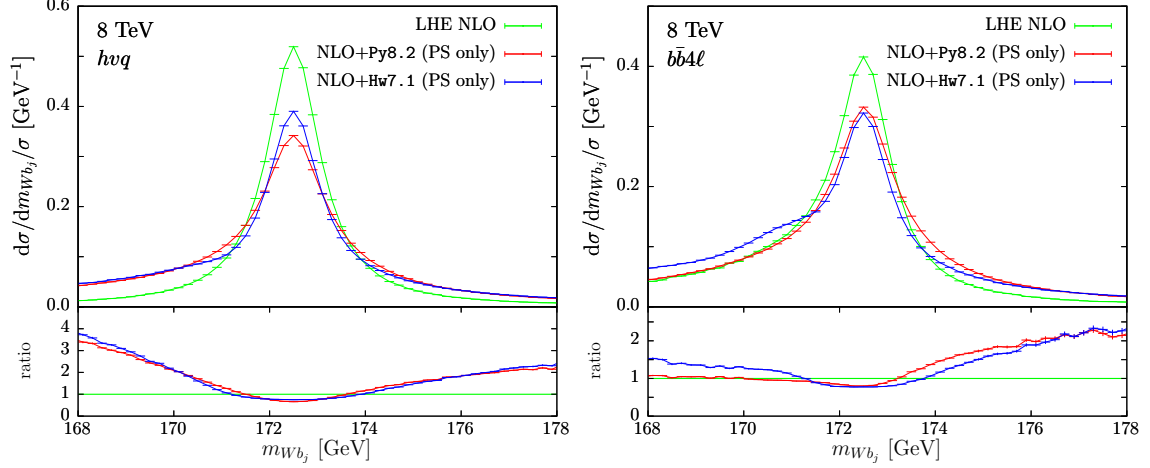


Figure 5. $d\sigma/dm_{Wb_j}$ distribution obtained with hvq (left pane) and $b\bar{b}4\ell$ (right pane) at the NLO LHE level (green), and at NLO+shower (in red *Pythia*8.2 and in blue *Herwig*7.1), normalized to 1 in the displayed range. In the bottom panel the ratio with the NLO LHE is shown.

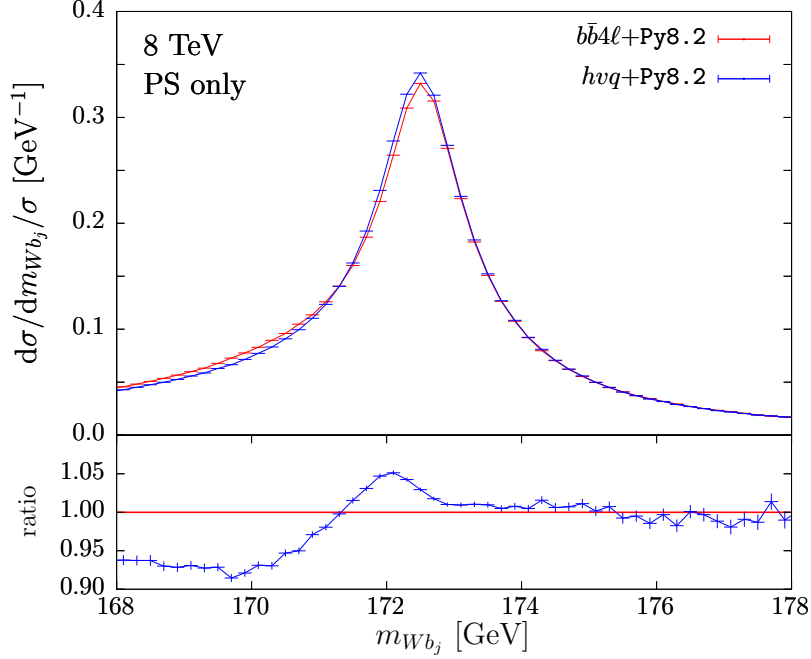


Figure 6. $d\sigma/dm_{Wb_j}$ distribution, normalized to 1 in the displayed range, obtained with $b\bar{b}4\ell$ (red) and hvq (blue) at the NLO+PS level using *Pythia*8.2.

peak. In fact, MPI-generated particles are deposited in the b -jet cone, thus increasing the b -jet energy. Hadronization widens the peak for both generators. However, in the *Pythia*8.2 case, we also observe a clear enhancement of the low mass region, that is not as evident in the *Herwig*7.1 case. In the combined effect of hadronization and MPI, *Herwig*7.1 has a wider peak. On the other hand, the high tail enhancement seems similar in the two generators.

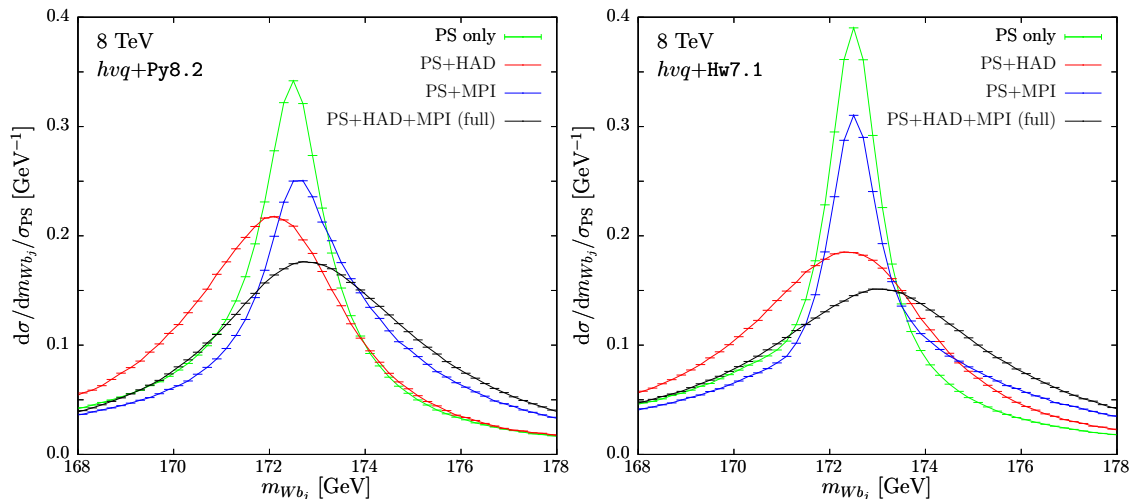


Figure 7. $d\sigma/dm_{Wb_j}$ distribution obtained with hvq interfaced with *Pythia*8.2 (left panel) and *Herwig*7.1 (right panel). In green, the NLO+PS results; in red, hadronization effects are included; in blue, NLO+PS with multi-parton interactions (MPI); and in black, with hadronization and MPI effects. The curves are normalized using the NLO+PS cross section in the displayed range.

We remark that the different mechanisms that lead to an increased cross section above and below the top peak depend on the jet radius parameter R . By increasing (or decreasing) R , the peak position is shifted to left (or right). Furthermore, differences in the implementation of radiation from the resonances, the hadronization model and the underlying events can also shift the peak, leading eventually to a displacement of the extracted top mass, that should be carefully assessed.

5 Methodology

In the following sections we will examine various sources of theoretical errors in the top-mass extraction, focusing upon three classes of observables: the reconstructed mass peak, the peak of the b -jet energy spectrum [27], and the leptonic observables of Ref. [28].

The reconstructed mass observable bears a nearly direct relation with the top mass. If two generators with the same m_t input parameter yield a reconstructed mass peak position that differ by a certain amount, we can be sure that if they are used to extract the top mass they will yield results that differ by roughly the same amount in the opposite direction. Of course, this is not the case for other observables. In general, for an observable O sensitive to the top mass, we will have

$$O = O_c + B(m_t - m_{t,c}) + \mathcal{O}\left((m_t - m_{t,c})^2\right), \quad (5.1)$$

where m_t is the input mass parameter in the generator, and $m_{t,c} = 172.5$ GeV is our reference central value for the top mass. O_c and B differ for different generators or generator setups. Given an experimental result for O , O_{exp} , the extracted mass value is

$$m_t = m_{t,c} + \frac{O_{\text{exp}} - O_c}{B}. \quad (5.2)$$

By changing the generator setup, O_c and B will assume the values O'_c and B' , and will yield a different extracted mass m'_t . We will thus have

$$m'_t - m_t = \frac{O_c - O'_c}{B} + (O_{\text{exp}} - O'_c) \frac{B - B'}{BB'}. \quad (5.3)$$

The second term is parametrically smaller, of one order higher in the deviation between the two generators, if we assume that at least one of them yields an m_t value sufficiently close to $m_{t,c}$. We thus have

$$m'_t - m_t \approx \frac{O_c - O'_c}{B}. \quad (5.4)$$

In practice, in the following, we will compute the B parameter using the *hvg* generator, that is the fastest one. We also checked that using the other generators for this purpose yields results that differ by at most 10%.

6 Reconstructed top mass distribution m_{Wb_j}

The peak of the reconstructed mass m_{Wb_j} , defined in Sec. 3.1, is a representative of all the direct measurement methods. Our simplifying assumptions, that the b jets are unambiguously identified and the neutrinos are fully reconstructed, including their sign, lead to an ideal resolution on the top peak that is not realistic. We thus compute these distributions also introducing a smearing that mimics the experimental systematics. This very crude approach allows us to concentrate more on theoretical issues rather than experimental ones. For example, if by using two different generators (or the same generator with different settings) we find differences in the extracted mass using our ideal m_{Wb_j} observable, we would be forced to conclude that there is an irreducible theoretical error (i.e. an error that cannot be reduced by increasing the experimental accuracy) on the mass measurement. The same problem in case of the smeared distribution should instead be considered less severe, since the corresponding error may be reduced if the experimental resolution is improved.

We remark that also “irreducible” errors (according to the definition given above) may in fact be reduced in practice. This is the case if one of the generators at hand does not fit satisfactorily measurable distributions related to top production. As an example, a generator may not fit reasonably the profile of the b jet, and we may be forced to change the allowed range for the parameters that control it, possibly reducing the error.

In the following, we will compare our three generators interfaced to *Pythia8.2*, and consider scale variation effects and PDF dependence. In order to investigate the sensitivity to the intensity of radiation from the b quark, we also consider different values of α_s as input. We will then investigate the *Herwig7.1* and *Pythia8.2* differences.⁸

It is quite obvious that the coefficient B of eq. (5.1) should be very near 1 for the m_{Wb_j} observable. The values for the B coefficients that we have obtained with the three generators showered with *Pythia8.2*, by a linear fit of the m_t dependence of the m_{Wb_j} distribution, are collected in Tab. 2, and confirm our expectation.

⁸Unless specified otherwise, *Pythia8.2* and *Herwig7.1* are setup to run in full hadron mode including shower, hadronization and multi-parton interactions.

	B , no smearing	B , smearing
$h\nu q$	1.002 ± 0.002	0.949 ± 0.001
$t\bar{t}dec$	1.000 ± 0.002	0.957 ± 0.001
$b\bar{b}4\ell$	1.008 ± 0.002	0.958 ± 0.001

Table 2. Values for the B coefficients of eq. (5.1) for the m_{Wb_j} peak position, for the non-smeared and smeared distributions (see Sec. 6.1 for details), obtained with the $h\nu q$, $t\bar{t}dec$ and $b\bar{b}4\ell$ generators showered with Pythia8.2.

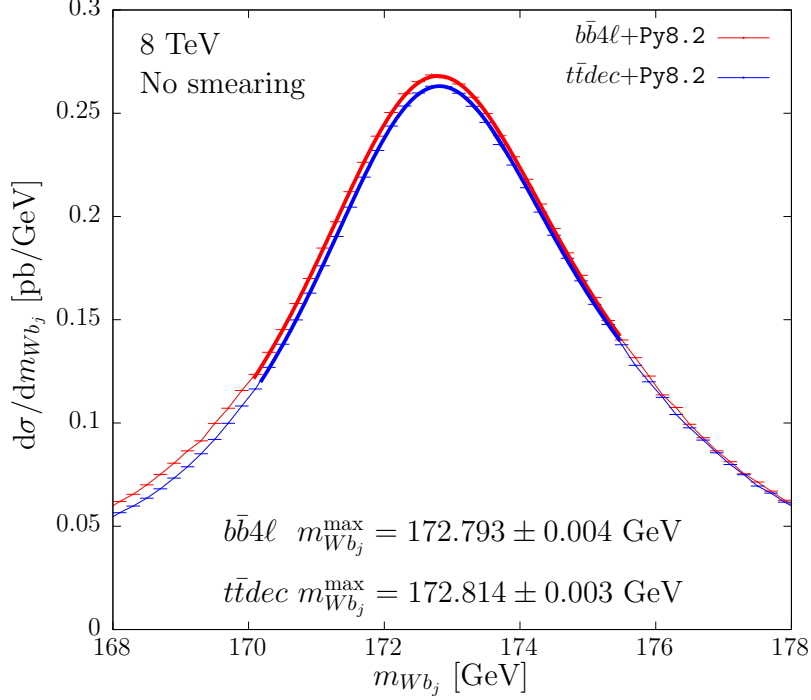


Figure 8. $d\sigma/dm_{Wb_j}$ distribution obtained with the $b\bar{b}4\ell$ and $t\bar{t}dec$ generators interfaced with Pythia8.2, for $m_t = 172.5$ GeV.

6.1 Comparison among the different NLO+PS generators

We begin by showing comparisons of our three generators, interfaced with Pythia8.2, for our reference top-mass value of 172.5 GeV. We show in Fig. 8 the m_{Wb_j} distribution for the $b\bar{b}4\ell$ and $t\bar{t}dec$ generators. We see that the two generators yield a very similar shape. We have extracted the position of the maximum by fitting the distribution with a skewed Lorentzian function of the form

$$y(m_{Wb_j}) = \frac{b[1 + d(m_{Wb_j} - a)]}{(m_{Wb_j} - a)^2 + c^2} + e. \quad (6.1)$$

The peak $m_{Wb_j}^{\max}$ is defined by

$$\left. \frac{dy(m_{Wb_j})}{dm_{Wb_j}} \right|_{m_{Wb_j} = m_{Wb_j}^{\max}} = 0. \quad (6.2)$$

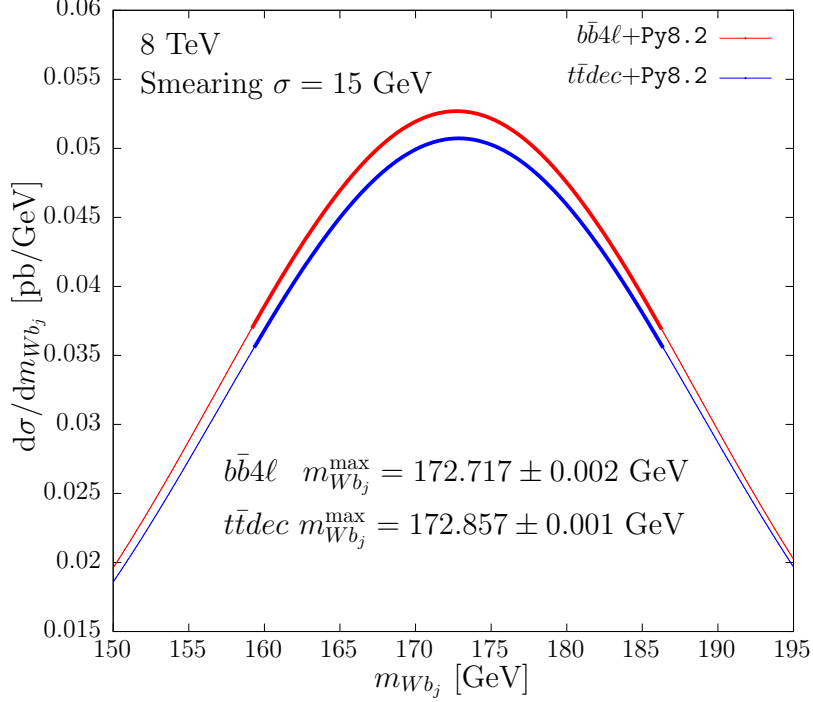


Figure 9. Smeared $d\sigma/dm_{Wb_j}$ distribution obtained with the $b\bar{b}4\ell$ and $t\bar{t}dec$ generators interfaced with Pythia8.2, for $m_t = 172.5$ GeV.

The fitting procedure is described in Appendix B.

As we can see from Fig. 8, the $b\bar{b}4\ell$ and $t\bar{t}dec$ results are very close to each other. We take this as an indication that interference effects in radiation and other off-shell effects, that are included in $b\bar{b}4\ell$ but not in $t\bar{t}dec$, have a very minor impact on the peak position, at least if we consider a measurement with an ideal resolution.

In order to mimic experimental resolution effects, we smear our distribution with a Gaussian of width $\sigma = 15$ GeV (that is the typical experimental resolution on the reconstructed top mass)

$$f_{\text{smeared}}(x) = \mathcal{N} \int dy f(y) \exp\left(-\frac{(y-x)^2}{2\sigma^2}\right), \quad (6.3)$$

where \mathcal{N} is a normalization constant. The results, obtained with the same fitting procedure, are shown in Fig. 9. Smearing effects are such that more importance is given to the region away from the peak, where there are larger differences between the two generators, leading to a difference in the peak position of 140 MeV.

In Figs. 10 and 11, we compare the $b\bar{b}4\ell$ and the $h\nu q$ generators in the non-smeared and smeared case respectively. We see a negligible differences in the peak position in the non-smeared case, while, in the smeared case, the $h\nu q$ generator differs from $b\bar{b}4\ell$ by -147 MeV, similar in magnitude to the case of $t\bar{t}dec$, but with opposite sign. These findings are summarized in Tab. 3, where we also include results obtained at the shower level.

We notice that $h\nu q$, in spite of the fact that it does not implement NLO corrections in top decay, yields results and distributions that are quite close to those of the most

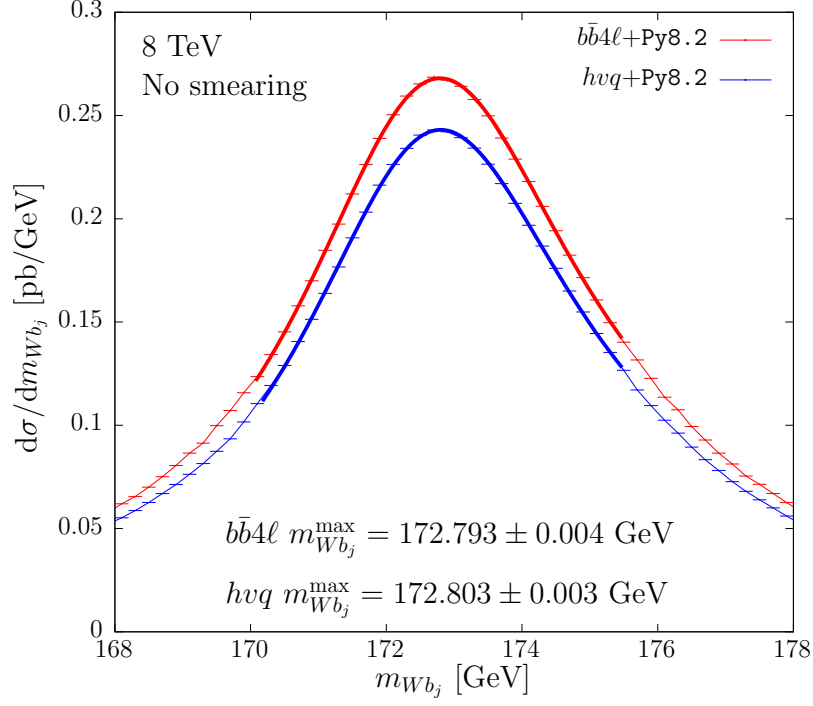


Figure 10. $d\sigma/dm_{Wb_j}$ distribution obtained with the $bb4l$ and hvq generators interfaced with Pythia8.2, for $m_t = 172.5$ GeV.

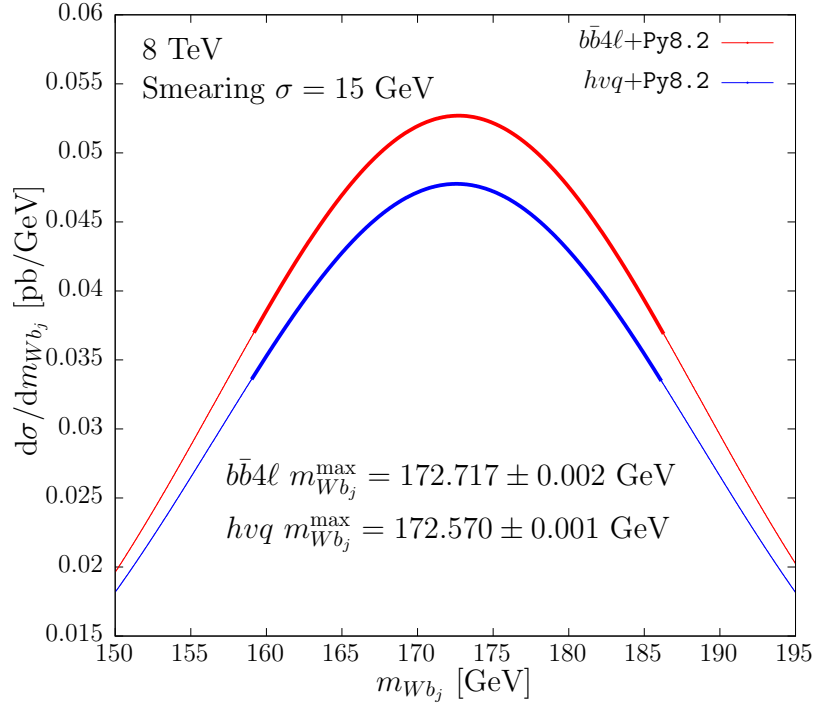


Figure 11. Smeared $d\sigma/dm_{Wb_j}$ distribution obtained with the $bb4l$ and hvq generators interfaced with Pythia8.2, for $m_t = 172.5$ GeV.

	PS only		full	
	No smearing	15 GeV smearing	No smearing	15 GeV smearing
$b\bar{b}4\ell$	172.522 ± 0.002 GeV	171.403 ± 0.002 GeV	172.793 ± 0.004 GeV	172.717 ± 0.002 GeV
$t\bar{t}dec - b\bar{b}4\ell$	-18 ± 2 MeV	$+191 \pm 2$ MeV	$+21 \pm 6$ MeV	$+140 \pm 2$ MeV
$h\nu q - b\bar{b}4\ell$	-24 ± 2 MeV	-89 ± 2 MeV	$+10 \pm 6$ MeV	-147 ± 2 MeV

Table 3. Differences in the m_{Wb_j} peak position for $m_t=172.5$ GeV for $t\bar{t}dec$ and $h\nu q$ with respect to $b\bar{b}4\ell$, showered with **Pythia8.2**, at the NLO+PS level and at the full hadron level.

	No smearing		15 GeV smearing	
	MEC	MEC – no MEC	MEC	MEC – no MEC
$b\bar{b}4\ell$	172.793 ± 0.004 GeV	-12 ± 6 MeV	172.717 ± 0.002 GeV	$+55 \pm 2$ MeV
$t\bar{t}dec$	172.814 ± 0.003 GeV	-4 ± 5 MeV	172.857 ± 0.001 GeV	-26 ± 2 MeV
$h\nu q$	172.803 ± 0.003 GeV	$+61 \pm 5$ MeV	172.570 ± 0.001 GeV	$+916 \pm 2$ MeV

Table 4. m_{Wb_j} peak position for $m_t=172.5$ GeV obtained with the three different generators, showered with **Pythia8.2**+MEC (default). We also show the differences between **Pythia8.2**+MEC and **Pythia8.2** without MEC.

accurate $b\bar{b}4\ell$ generator. This is due to the fact that **Pythia8.2** includes matrix-element corrections (MEC) in top decay by default, and MEC are equivalent, up to an irrelevant normalization factor, to next-to-leading order corrections in decay. This observation is confirmed by examining, in Tab. 4, the impact of the MEC setting on our predictions. When MEC are switched off, we see a considerable shift, near 1 GeV, in the $h\nu q$ result for the peak position in the smeared distribution, and a very minor one in the $b\bar{b}4\ell$ and $t\bar{t}dec$ generators, that include the hardest emission off b quarks. Thus, we conclude that the MEC in **Pythia8.2** do a decent job in simulating top decay as far as the m_{Wb_j} distribution is concerned. The remaining uncertainty of roughly 140 MeV in the case of both $h\nu q$ and $t\bar{t}dec$ generators, pulling in opposite directions, is likely due to the approximate treatment of off-shell effects.

6.1.1 Renormalization- and factorization-scale dependence

In this section, we study the dependence of our results on the renormalization and factorization scales (μ_R and μ_F), that gives an indication of the size of higher-orders corrections. We varied μ_R and μ_F around the central scale μ defined in eqs. (3.1) and (3.3) according to

$$\mu_R = K_R \mu, \quad \mu_F = K_F \mu, \quad (6.4)$$

where (K_R, K_F) are varied over the following combinations

$$\left\{ (1, 1), (2, 2), \left(\frac{1}{2}, \frac{1}{2} \right), (1, 2), \left(1, \frac{1}{2} \right), (2, 1), \left(\frac{1}{2}, 1 \right) \right\}. \quad (6.5)$$

We take $K_R = K_F = 1$ as our central prediction. We find that for $b\bar{b}4\ell$ there is a non-negligible scale dependence, that in the smeared case yields a theoretical uncertainty

of $^{+86}_{-53}$ MeV. For $t\bar{t}dec$ and hvq this uncertainty is smaller than 7 MeV. This is due to the fact that, in the last two generators, the NLO corrections are performed for on-shell tops, and the top width is subsequently generated with a smearing procedure. Thus, NLO corrections remain constant around the top peak, leading to a constant scale dependence. This leads to an underestimate of scale uncertainties in $t\bar{t}dec$ and hvq .

6.1.2 PDF set dependence

We evaluated the dependence from the PDFs by considering the central member of the following PDF sets:

- MSTW2008nlo68c1 ($\alpha_s(m_Z) = 0.120179$) (default) [56],
- PDF4LHC15_nlo_30_pdfas ($\alpha_s(m_Z) = 0.118$) [59],
- CT14nlo ($\alpha_s(m_Z) = 0.118$) [60],
- MMHT2014nlo68c1 ($\alpha_s(m_Z) = 0.120$) [61],
- NNPDF30_nlo_as_0118 ($\alpha_s(m_Z) = 0.118$) [62].

We generated the events by using the MSTW2008nlo68c1 set, and obtained all other predictions using the internal reweighting facility of the POWHEG BOX. We find that the corresponding differences in the m_{Wb_j} peak position are typically below 9 MeV and the variations are very similar for all the NLO+PS generators.

We also generated a sample using the central parton-distribution function of the PDF4LHC15_nlo_30_pdfas set, and, by reweighting, all its members, within the hvq generator. In this case, our error is given by the sum in quadrature of all deviations. We get a variation of 3 MeV in the non-smear case, and 5 MeV for the smeared distribution. We find that the variation band obtained in this way contains the central value results for the different PDF sets that we have considered. It thus makes sense to use this procedure for the estimate of PDF uncertainties. On the other hand, reweighting for the 30 members of the set in the $b\bar{b}4\ell$ case is quite time consuming, since the virtual corrections are recomputed for each weight. We thus assume that the PDF uncertainties computed in the hvq case are also valid for the $b\bar{b}4\ell$ and $t\bar{t}dec$ cases, since the dependence on the PDF is mostly due to the implementation of the production processes, and all our generators describe it at NLO accuracy, and since we have previously observed that by reweighting to several PDF sets we get very similar variations for all generators.

In general, PDF uncertainties are rather small. This is probably due to the fact that, in order to shift the position of the peak, some differences must be present in the modeling of final-state radiation (FSR). These differences may arise from differences in α_s . However, reweighting in POWHEG only affects the inclusive cross section, and not the radiation, and thus final-state radiation is not modified by these changes.

6.1.3 Strong-coupling dependence

In POWHEG BOX the scale used to generate the emissions is the transverse momentum of the radiation (with respect to the emitter). At the moment, facilities to study uncertainties due

to variations of this scheme are not available. On the other hand, these uncertainties would lead to a different radiation pattern around the b jet, that can in turn have a non-negligible effect on the reconstructed mass.

The simplest way at our disposal for studying the sensitivity of the reconstructed mass on the intensity of radiation from the b quark is by varying the value of α_s . To this end we use the `NNPDF30_nlo_as115` and `NNPDF30_nlo_as121` sets, where $\alpha_s(m_Z)=0.115$ and $\alpha_s(m_Z)=0.121$, respectively. As stated earlier, we cannot use the `POWHEG` reweighting facility in order to study this effect, and thus we generated two dedicated samples (see Tab. 1).

We found that the extracted peak positions in the smeared m_{Wb_j} distributions for the two extreme values of α_s differ by 128 MeV for the $b\bar{b}4\ell$ generator, by 108 MeV for the $t\bar{t}dec$ generator and by 18 MeV for $h\nu q$. The small α_s -sensitivity in the $h\nu q$ case is expected, since, in this case, radiation in decays is handled by the shower, and thus should be studied by varying shower parameters. In the $b\bar{b}4\ell$ and $t\bar{t}dec$ case, the variation is very similar, since they both include NLO radiation in decay, and the direction of the variation is as expected, i.e. the peak position is larger for the smaller α_s value, due to the reduced loss of energy outside the jet cone. Differences in the case of non-smeared distributions are in all cases not larger than 8 MeV.

We can estimate the typical scale of radiation in top decay as being of the order of 30 GeV, i.e. one-half of the typical b energy in the top rest frame. The ratio of the upper to lower $\alpha_s(m_Z)$ values that we have consider is 1.052, and it becomes 1.06 at a scale of 30 GeV. On the other hand, a scale variation of a factor of two above and below 30 GeV yields a variation in α_s of about 26%. This can be taken as a rough indication that a standard scale variation would yield to a variation in the peak position that is more than a factor four larger than the one obtained by varying α_s .

6.1.4 Matching uncertainties

The `FSREmission` veto procedure (i.e. implementation 1 of Sec. 2.1.2) represents the most accurate way to perform the vetoed shower on the `POWHEG BOX` generated events, because it uses the `POWHEG` definition of transverse momentum rather than the `Pythia8.2` one. The `ScaleResonance` procedure (i.e. method 2) introduces a mismatch (see Sec. 2.1.2) that we take as an indication of the size of the matching uncertainties. The extracted peak position for the $b\bar{b}4\ell$ and $t\bar{t}dec$ with the two matching procedures are summarized in Tab. 5. We can see that these differences are roughly 20 MeV in $b\bar{b}4\ell$ for both the no-smearing and smearing case, and in $t\bar{t}dec$ they are a few MeV for the no-smearing case, and 20 MeV with smearing. When using the generic veto method of Sec. 2.1.1 we find differences of comparable size.

6.1.5 Summary of scale, PDF and α_s variations

In Tab. 6 we summarize the uncertainties due to scale, PDF and strong-coupling variations, connected with the extraction of the m_{Wb_j} peak position, for the input mass $m_t = 172.5$ GeV, for all the generators showered with `Pythia8.2`.

	No smearing		15 GeV smearing	
	SR	SR – FSR	SR	SR – FSR
$b\bar{b}4\ell$	172.816 ± 0.004 GeV	$+23 \pm 6$ MeV	172.737 ± 0.002 GeV	20 ± 2 MeV
$t\bar{t}dec$	172.812 ± 0.004 GeV	-1 ± 5 MeV	172.878 ± 0.001 GeV	21 ± 2 MeV

Table 5. m_{Wb_j} peak position for $m_t=172.5$ GeV obtained with the $b\bar{b}4\ell$ and $t\bar{t}dec$ generators, showered with Pythia8.2, for the ScaleResonance (SR) veto procedure. The differences with FSREmission (FSR), that is our default, are also shown.

	No smearing				15 GeV smearing			
	% – $b\bar{b}4\ell$	(μ_R, μ_F)	PDF	α_s	% – $b\bar{b}4\ell$	(μ_R, μ_F)	PDF	α_s
$b\bar{b}4\ell$	+0 MeV	$^{+26}_{-17}$ MeV	-	± 8 MeV	+0 MeV	$^{+86}_{-53}$ MeV	-	± 64 MeV
$t\bar{t}dec$	+21 MeV	$^{+2}_{-10}$ MeV	-	± 8 MeV	+140 MeV	$^{+6}_{-6}$ MeV	-	± 54 MeV
$h\nu q$	+10 MeV	$^{+2}_{-6}$ MeV	± 3 MeV	± 2 MeV	-147 MeV	$^{+7}_{-7}$ MeV	± 5 MeV	± 9 MeV

Table 6. Theoretical uncertainties associated with the m_{Wb_j} peak position extraction for $m_t=172.5$ GeV for the three different generators, showered with Pythia8.2. The PDF uncertainty on the $b\bar{b}4\ell$ and $t\bar{t}dec$ generators is assumed to be equal to the $h\nu q$ one, as explained in Sec. 6.1.2.

The upper (lower) error due to scale variation reported in the table is obtained by taking the maximum (minimum) position of the m_{Wb_j} peak for each of the seven scales choices of eq. (6.5), minus the one obtained for the central scale.

In the PDF case, as discussed in Sec. 6.1.2, we compute the PDF uncertainties only for the $h\nu q$ generator, and assume that they are the same for $b\bar{b}4\ell$ and $t\bar{t}dec$.

We consider a symmetrized strong-coupling dependence uncertainty, whose expression is given by

$$\delta m_{Wb_j}(\alpha_s(m_Z)) = \pm \frac{|m_{Wb_j}(0.115) - m_{Wb_j}(0.121)|}{2}. \quad (6.6)$$

We stress that these variation have only an indicative meaning. In a realistic analysis, experimental constraints may reduce these uncertainties. We also stress that these are not the only theoretical uncertainties. Others may be obtained by varying Monte Carlo parameters. Here we focus specifically on those uncertainties that are associated with the NLO+PS generators.

As we have already discussed, the use of the $h\nu q$ and the $t\bar{t}dec$ generators would lead to a negligible bias in the m_{Wb_j} distribution if we were able to measure it without any resolution effects. However, if we introduce a smearing to mimic them, the description of the region away from the peak plays an important role, and the $h\nu q$ and $t\bar{t}dec$ generators yield predictions for the mass peak position that are shifted by roughly 140 MeV in the downward and upward direction respectively with respect to $b\bar{b}4\ell$.

We also notice that the $b\bar{b}4\ell$ generator is the most affected by theoretical uncertainties. In particular, the $t\bar{t}dec$ and $h\nu q$ generators have an unrealistically small scale dependence of the peak shape, due to the way in which off-shell effects are approximately described.

	$R = 0.4$		$R = 0.5$		$R = 0.6$	
	No smearing	15 GeV smearing	No smearing	15 GeV smearing	No smearing	15 GeV smearing
$b\bar{b}4\ell$ [GeV]	172.156 ± 0.004	171.018 ± 0.002	172.793 ± 0.004	172.717 ± 0.002	173.436 ± 0.005	174.378 ± 0.002
$t\bar{t}dec - b\bar{b}4\ell$	$+35 \pm 5$ MeV	$+195 \pm 2$ MeV	$+21 \pm 6$ MeV	$+140 \pm 2$ MeV	$+1 \pm 7$ MeV	$+97 \pm 2$ MeV
$h\nu q - b\bar{b}4\ell$	$+47 \pm 5$ MeV	-113 ± 2 MeV	$+10 \pm 6$ MeV	-147 ± 2 MeV	-7 ± 6 MeV	-174 ± 2 MeV

Table 7. m_{Wb_j} peak position obtained with the $b\bar{b}4\ell$ generator for three choices of the jet radius. The differences with the $t\bar{t}dec$ and the $h\nu q$ generators are also shown.

The $t\bar{t}dec$ generator displays a non-negligible sensitivity only to the strong-coupling constant. The theoretical errors that we have studied here lead to very small effects for the $h\nu q$ generator, since it does not include radiative corrections in the top decay. On the other hand, the $h\nu q$ generator is bound to be more sensitive to variation of parameters in Pythia8.2, that in this case fully controls the radiation from the b quark.

6.1.6 Radius dependence

In this section we investigate the stability of the previous results with respect to the choice of the jet radius. The results are summarized in Tab. 7. For the distributions without smearing, the differences between the three generators are small and decrease as R increases. For the smeared distributions, the differences between $t\bar{t}dec$ and $b\bar{b}4\ell$ decrease as the radius increase, while the difference between the $h\nu q$ and the $b\bar{b}4\ell$ generator increases.

The small differences in R dependence among the three generators in the non-smeared case can be understood if we consider that differences in the b radiation do not affect much the peak position in the non-smeared distribution, but rather they affect the strength of the tail on the left side of the peak. On the other hand, the peak position is affected by radiation in production and by the underlying-event structure, that is very similar in the three generators.

It should be noticed that the difference between the displacements of the $t\bar{t}dec$ and $h\nu q$ with respect to $b\bar{b}4\ell$ is less than 55 MeV and 34 MeV, respectively, below the current statistical precision of top-mass measurements. Thus, the good agreement found among the three generators persists also for different R values.

6.2 Comparison with Herwig7.1

In order to assess uncertainties due to the showering program, in this section we compare the results obtained using Herwig7.1 and Pythia8.2. In Tab. 8 we compare the m_{Wb_j} peak position extracted for the input mass $m_t = 172.5$ GeV using the three generators showered with Pythia8.2 and Herwig7.1. For the $h\nu q$ generator, the differences are of the order of 240 MeV for both the smeared and non-smeared case, but with opposite signs. In the smeared case, both the $t\bar{t}dec$ and $b\bar{b}4\ell$ generators yield much larger differences, of more than 1 GeV.

In Tab. 9 we report the differences between the Herwig7.1 and Pythia8.2 predictions for all the generators, at the NLO+PS level and at the full hadron level. We notice that at the NLO+PS level and without smearing, the differences between the two parton-shower

	No smearing		15 GeV smearing	
	Hw7.1	Py8.2 – Hw7.1	Hw7.1	Py8.2 – Hw7.1
$b\bar{b}4\ell$	172.727 ± 0.005 GeV	$+66 \pm 7$ MeV	171.626 ± 0.002 GeV	$+1091 \pm 2$ MeV
$t\bar{t}dec$	172.775 ± 0.004 GeV	$+39 \pm 5$ MeV	171.678 ± 0.001 GeV	$+1179 \pm 2$ MeV
$h\nu q$	173.038 ± 0.004 GeV	-235 ± 5 MeV	172.319 ± 0.001 GeV	$+251 \pm 2$ MeV

Table 8. m_{Wb_j} peak position for $m_t=172.5$ GeV obtained with the three different generators, showered with **Herwig7.1** (Hw7.1). The differences with **Pythia8.2** (Py8.2) are also shown.

	Pythia8.2 – Herwig7.1			
	PS only		full	
	No smearing	15 GeV smearing	No smearing	15 GeV smearing
$b\bar{b}4\ell$	$+10 \pm 2$ MeV	$+984 \pm 2$ MeV	$+66 \pm 7$ MeV	$+1091 \pm 2$ MeV
$t\bar{t}dec$	$+5 \pm 2$ MeV	$+1083 \pm 2$ MeV	$+39 \pm 5$ MeV	$+1179 \pm 2$ MeV
$h\nu q$	-0 ± 2 MeV	$+113 \pm 2$ MeV	-235 ± 5 MeV	$+251 \pm 2$ MeV

Table 9. Differences between **Pythia8.2** and **Herwig7.1** in the extracted m_{Wb_j} peak position for $m_t=172.5$ GeV obtained with the three different generators, at the NLO+PS level (PS only) and including also the underlying events, the multi-parton interactions and the hadronization (full).

	Pythia8.2 – Herwig7.1					
	$R = 0.4$		$R = 0.5$		$R = 0.6$	
	No smearing	15 GeV smearing	No smearing	15 GeV smearing	No smearing	15 GeV smearing
$b\bar{b}4\ell$	-98 ± 7 MeV	$+830 \pm 2$ MeV	$+66 \pm 7$ MeV	$+1091 \pm 2$ MeV	$+253 \pm 8$ MeV	$+1267 \pm 2$ MeV
$t\bar{t}dec$	-100 ± 5 MeV	$+979 \pm 2$ MeV	$+39 \pm 5$ MeV	$+1179 \pm 2$ MeV	$+210 \pm 6$ MeV	$+1314 \pm 2$ MeV
$h\nu q$	-370 ± 5 MeV	$+73 \pm 2$ MeV	-235 ± 5 MeV	$+251 \pm 2$ MeV	-31 ± 6 MeV	$+389 \pm 2$ MeV

Table 10. Differences in the m_{Wb_j} peak position obtained matching the three generators with **Pythia8.2** and **Herwig7.1**, for three choices of the jet radius.

programs are negligible. For the smeared distributions, at both the NLO+PS and full level, the differences are roughly 1 GeV for the $b\bar{b}4\ell$ and the $t\bar{t}dec$ generator. For $h\nu q$ the differences are considerably smaller, although not quite negligible. Furthermore, accidental compensation effects seem to emerge in this case if we compare the peak displacement in the distributions with and without smearing.

The origin of these large differences are better understood by looking at the differential cross sections plotted in Figs. 12 and 13. In Fig. 12 we plot the results for the non-smeared case, at the NLO+PS level (left) and at the full hadron level (right): while the peak position is nearly the same for both **Pythia8.2** and **Herwig7.1**, the shape of the curves is very different around the peak, leading to a different mass peak position when smearing is applied, as displayed in Fig. 13. We notice that in this last case we see a difference in shape also after smearing. This suggests that at least one of the two generators may not

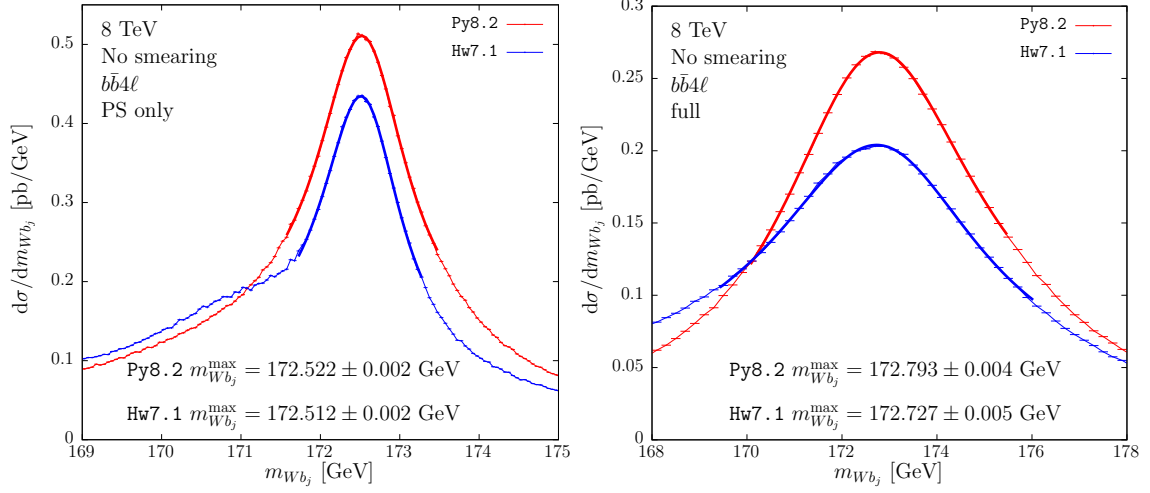


Figure 12. $d\sigma/dm_{Wb_j}$ distribution obtained by showering the $b\bar{b}4\ell$ results with Pythia8.2 and Herwig7.1, at parton-shower level (left) and with hadronization and underlying events (right).

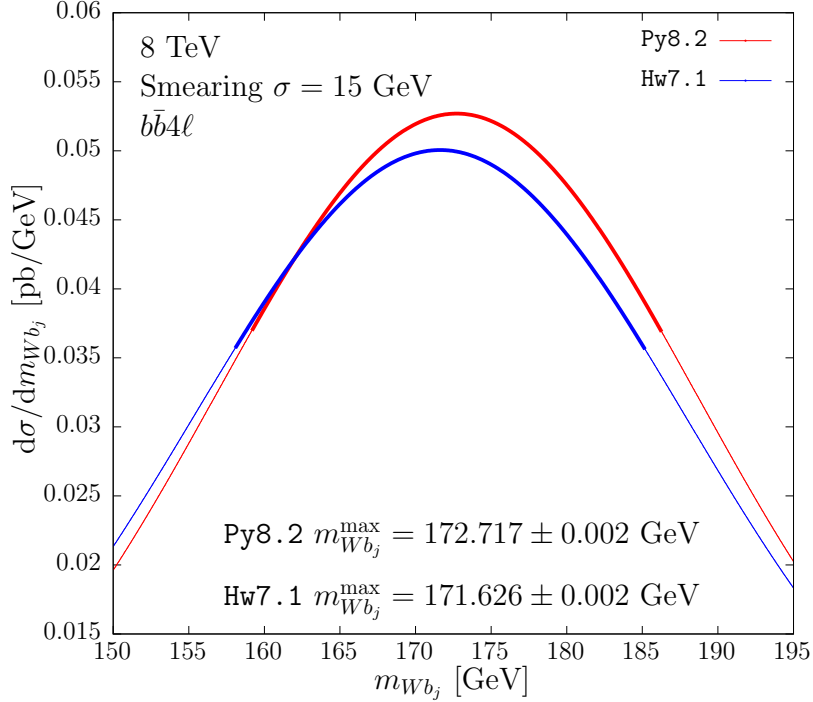


Figure 13. Smeared $d\sigma/dm_{Wb_j}$ distribution obtained by matching the $b\bar{b}4\ell$ generator with Pythia8.2 and Herwig7.1.

describe the data fairly.

Since we observe such large differences in the value of $m_{Wb_j}^{\max}$ in Herwig7.1 and Pythia8.2, we have also studied whether sizable differences are also present in the $m_{Wb_j}^{\max}$ dependence upon the jet radius R . The results are shown in Tab. 10, and displayed in Fig. 14. In the case of the $b\bar{b}4\ell$ generator, the difference between Pythia8.2 and Herwig7.1 goes from 830

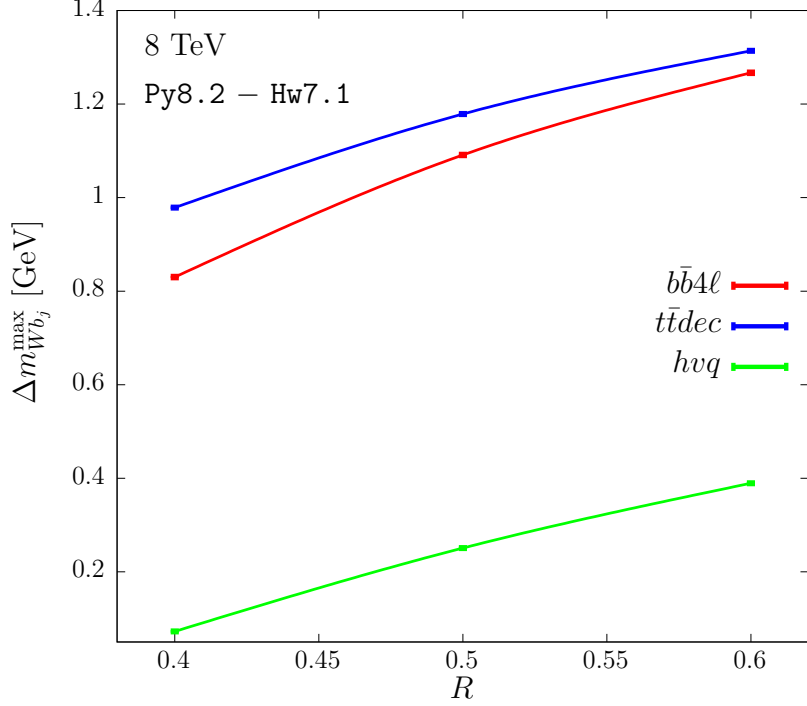


Figure 14. Differences of $m_{Wb_j}^{\max}$ between the Pythia8.2 and the Herwig7.1 showers, for the three generators, as a function of the jet radius.

to 1267 MeV. Thus, assuming for instance that Pythia8.2 fits the data perfectly, i.e. that it extracts the same value of the mass by fitting the $m_{Wb_j}^{\max}$ values obtained with the three different values of R , Herwig7.1 would extract at $R = 0.6$ a mass value that is larger by 437 MeV from the one extracted at $R = 0.4$. We stress that the differences in R behaviour of $m_{Wb_j}^{\max}$ may have the same origin as the difference in the reconstructed mass value, since both effects may be related to the amount of energy that enters the jet cone, and it is not unlikely that, by tuning one the two generators in such a way that they both have the same R dependence, also their difference in $m_{Wb_j}^{\max}$ would be reduced.⁹ Thus, the differences that we find in the present work do not necessarily translate into an uncertainty in the extracted mass value, since they may be reduced by requiring that the generators represent the data fairly.

6.2.1 Alternative matching prescriptions in Herwig7.1

We have examined several variations in the Herwig7.1 settings, and in the interface between POWHEG and Herwig7.1, in order to understand whether the Herwig7.1 results are reasonably stable, or depend upon our particular settings.

⁹Similarly, one could fit appropriate calibration observables associated to the b -jet structure, along the lines of Ref. [63].

hvq	No smearing	15 GeV smearing
MEC – no MEC	307 ± 6 MeV	1371 ± 2 MeV
MEC – POWHEG	244 ± 6 MeV	356 ± 2 MeV

Table 11. Differences in the m_{Wb_j} peak position for the hvq generator showered with **Herwig7.1**, with MEC switched off (no MEC) or using the **Herwig7.1** POWHEG option, with respect to our default setting, that has MEC switched on.

	No smearing		15 GeV smearing	
	FSV	FSV – SV	FSV	FSV – SV
$b\bar{b}4\ell$	172.776 ± 0.005 GeV	$+49 \pm 7$ MeV	171.829 ± 0.002 GeV	$+203 \pm 2$ MeV
$t\bar{t}dec$	172.810 ± 0.004 GeV	$+35 \pm 6$ MeV	171.906 ± 0.001 GeV	$+228 \pm 2$ MeV

Table 12. m_{Wb_j} peak position for $m_t=172.5$ GeV for $b\bar{b}4\ell$ and $t\bar{t}dec$ showered with **Herwig7.1** using the **FullShowerVeto** (FSV) procedure. The differences with **ShowerVeto** (SV), that represents our default, are also shown.

MEC and POWHEG options in Herwig7.1

In **Herwig7.1**, matrix-element corrections are active by default, but **Herwig7.1** offers also the possibility to switch them off. In addition, it allows to optionally replace the MEC with its internal POWHEG method, when available, to achieve NLO accuracy in top decays.¹⁰ We have verified that, as expected, switching off the matrix-element corrections does not significantly affect the $b\bar{b}4\ell$ and $t\bar{t}dec$ results. In the case of the hvq generator, we can compare the default case, where MEC is on, with the cases where POWHEG replaces MEC, and with the case where neither MEC nor POWHEG is implemented. The results are shown in Tab. 11. We notice that the inclusion of MEC enhances by more than 1.3 GeV the peak position of the smeared distribution. A similar result was found in **Pythia8.2** (see Tab. 4), where the difference was slightly less than 1 GeV. The difference between the POWHEG and MEC results is much below the 1 GeV level but not negligible. This fact is hard to understand, since the POWHEG and MEC procedures should only differ by a normalization factor.

Alternative veto procedures in Herwig7.1

As discussed in Sec. 2.1.3, **Herwig7.1** offers two different classes that implement the veto procedure: the **ShowerVeto**, our default one, and the **FullShowerVeto** class. The corresponding results are summarized in Tab. 12. For both the $b\bar{b}4\ell$ and the $t\bar{t}dec$ the two procedures lead to a 200 MeV difference in the peak position for the smeared distributions. The origin of such difference is not fully clear to us. In part it may be ascribed to the fact that when using the **ShowerVeto** class we mix two different definitions of transverse momentum (the **Herwig7.1** and the POWHEG one), and in part may be due to the fact

¹⁰These options are activated by the instructions `set ShowerHandler:HardEmission None` or `set ShowerHandler:HardEmission POWHEG`, respectively.

	No smearing		15 GeV smearing	
	TS	TS – default	TS	TS – default
$b\bar{b}4\ell$	$172.730 \pm 0.005 \text{ GeV}$	$+3 \pm 8 \text{ MeV}$	$171.496 \pm 0.002 \text{ GeV}$	$-130 \pm 2 \text{ MeV}$
$t\bar{t}dec$	$172.786 \pm 0.004 \text{ GeV}$	$+12 \pm 6 \text{ MeV}$	$171.546 \pm 0.001 \text{ GeV}$	$-132 \pm 2 \text{ MeV}$

Table 13. m_{Wb_j} peak position for $m_t=172.5 \text{ GeV}$ obtained with the $b\bar{b}4\ell$ and $t\bar{t}dec$ generators showered with **Herwig7.1**, with the settings of eq. (6.7) (labelled as TS). The differences with the default results are also shown.

that in the **FullShowerVeto** class the vetoing is done on the basis of the shower structure after reshuffling has been applied. We have also checked that the generic procedure of Sec. 2.1.1, although much slower, leads to results that are statistically compatible with the **FullShowerVeto** method.

Truncated showers

It was shown in Ref. [36] that, when interfacing a **POWHEG** generator to an angular ordered shower, in order to compensate for the mismatch between the angular order scale and the **POWHEG** hardness, that is taken equal to the relative transverse momentum in radiation, one should supply appropriate truncated showers. None of our vetoing algorithms take them into account, but it turns out that **Herwig7.1** provides facilities to change the settings of the initial showering scale according to the method introduced in Ref. [64], that, in our case, are equivalent to the inclusion of truncated showers (see Appendix D). This is done by inserting the following instructions in the **Herwig7.1** input file:

$$\begin{aligned} \text{set PartnerFinder:PartnerMethod Maximum} \\ \text{set PartnerFinder:ScaleChoice Different.} \end{aligned} \tag{6.7}$$

The effects of these settings for the $b\bar{b}4\ell$ and $t\bar{t}dec$ generators are shown in Tab. 13. The inclusion of the truncated shower does not introduce dramatic changes in the peak position: in fact the differences are negligible in the distributions without smearing, and are roughly 130 MeV when smearing is applied. It should be noticed that these settings slightly increase the difference with respect to the results obtained with **Pythia8.2**.

7 The energy of the b jet

In Ref. [27] it was proposed to extract m_t using the peak of the energy spectrum of the b jet. At leading order, the b jet consists of the b quark alone, and its energy in the top rest frame, neglecting top-width effects, is fixed and given by

$$E_{b_j}^{\text{max}} = \frac{m_t^2 - m_W^2 + m_b^2}{2m_t}, \tag{7.1}$$

i.e. the spectrum is a delta function in the energy. In the laboratory frame, because of the variable boost that affects the top, the delta function is smeared into a wider distribution,

but it can be shown that its peak position remains at $E_{b_j}^{\max}$. On the basis of this observation we are led to assume that also after the inclusion of off-shell effects, radiative and non-perturbative corrections, the relation between $E_{b_j}^{\max}$ and the top pole-mass m_t should be largely insensitive to production dynamics.

We performed a study of the $E_{b_j}^{\max}$ observable along the same lines adopted for m_{Wb_j} in the previous section. If the range of variations of the top mass around a given central value $m_{t,c}$ is small enough, a linear relation between $E_{b_j}^{\max}$ and the top mass must hold, so that we can write

$$E_{b_j}^{\max}(m_t) = E_{b_j}^{\max}(m_{t,c}) + B(m_t - m_{t,c}) + \mathcal{O}(m_t - m_{t,c})^2. \quad (7.2)$$

It was suggested in Ref. [33] that the E_{b_j} distribution $d\sigma/dE_{b_j}$ is better fitted in terms of $\log E_{b_j}$. Thus, in order to extract the peak position, we fitted the energy distribution with a fourth order polynomial

$$y = a + b(x - x^{\max})^2 + c(x - x^{\max})^3 + d(x - x^{\max})^4, \quad (7.3)$$

where $x = \log E_{b_j}$.

The parameter B of eq. (7.2), extracted from a linear fit of the three $E_{b_j}^{\max}$ values corresponding to the three different values of m_t that we have considered (see Tab. 1) using the *hvg* generator showered by *Pythia8.2*, was found to be

$$B = 0.50 \pm 0.03, \quad (7.4)$$

compatible with the expected value of 0.5 from eq. (7.1).¹¹

7.1 Comparison among different NLO+PS generators

In Fig. 15 we plot the logarithmic energy distribution for the three generators interfaced to *Pythia8*, together with their polynomial fit. The extracted E_{b_j} peaks from the $b\bar{b}4\ell$ and the $t\bar{t}dec$ generators are compatible within the statistical errors. On the other hand, the *hvg* generator yields a prediction which is roughly 460 ± 100 MeV smaller than the $b\bar{b}4\ell$ one. We thus observe that the jet modeling implemented by *Pythia8.2* with MEC seems to yield slightly less energetic jets. An effect going in the same direction was also observed for the m_{Wb_j} observable (see Tab. 6, the first column of the results with smearing), although to a smaller extent.

In Tab. 14 we have collected the values of $E_{b_j}^{\max}$ computed with MEC, and the differences between the results with and without MEC. We notice that the MEC setting has little impact in the $b\bar{b}4\ell$ and $t\bar{t}dec$ cases. On the other hand, in the *hvg* case the absence of MEC would have lead to an $E_{b_j}^{\max}$ value about 2 GeV smaller than with MEC. We take this as another indication that the implementation of radiation in top decay using MEC leads to results that are much closer to the NLO+PS ones.

In Tab. 15 we summarize our results together with the scale, PDF and α_s uncertainties,

¹¹When using the $b\bar{b}4\ell$ generator we obtain $B = 0.54 \pm 0.07$, while with the $t\bar{t}dec$ one, we get $B = 0.50 \pm 0.03$. When using *Herwig7.1* instead of *Pythia8.2*, we find values compatible with the given ones within 10%.

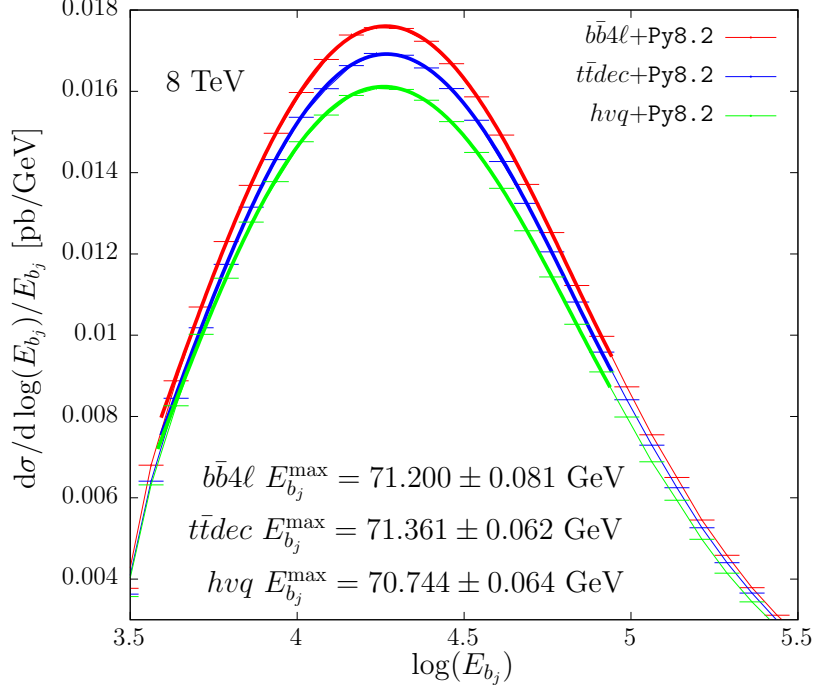


Figure 15. Logarithmic energy distribution obtained with the three generators interfaced to `Pythia8`, together with their polynomial fit, in the range displayed in the figure. The value of $E_{b_j}^{\max}$ for each generator is also reported.

	MEC	MEC – no MEC
$b\bar{b}4\ell$	71.200 ± 0.081 GeV	$+170 \pm 115$ MeV
$t\bar{t}dec$	71.361 ± 0.062 GeV	-69 ± 87 MeV
$h\nu q$	70.744 ± 0.064 GeV	$+1937 \pm 92$ MeV

Table 14. E_{b_j} peak position obtained with the three generators showered with `Pythia8.2`. The differences between the peak positions extracted by switching on and off the matrix-element corrections are also shown.

	% – $b\bar{b}4\ell$	(μ_R, μ_F)	PDF	α_s	stat
$b\bar{b}4\ell$	+0 MeV	$^{+22}_{-15}$ MeV	-	± 35 MeV	± 81 MeV
$t\bar{t}dec$	+161 MeV	$^{+22}_{-24}$ MeV	-	± 17 MeV	± 62 MeV
$h\nu q$	-456 MeV	$^{+32}_{-47}$ MeV	± 30 MeV	± 25 MeV	± 64 MeV

Table 15. Theoretical uncertainties for the E_{b_j} peak position obtained with the three generators showered with `Pythia8.2`. The last column reports the statistical uncertainty of our results.

that are extracted with a procedure analogous to one described for the m_{Wb_j} observable. We also report the corresponding statistical errors of our results. We see that scale and PDF variations have negligible impact on our observable, the only important change being

associated with the choice of the NLO+PS generator.

We notice that our errors on scale and PDF variations are much smaller than our statistical errors. On the other hand, these variations are performed by reweighting techniques, that, because of correlations, lead to errors in the differences that are much smaller than the error on the individual term. In view of the small size of these variations, we do not attempt to perform a better estimate of their error. On the other hand, the variation of α_s do not benefit of this cancellation, and are all below the statistical uncertainties.

As previously done for m_{Wb_j} , we have also investigated the dependence of the b -jet peak positions on the jet radius. The results are summarized in Tab. 16. While we observe

	$R = 0.4$	$R = 0.5$	$R = 0.6$
$b\bar{b}4\ell$	$67.792 \pm 0.089 \text{ GeV}$	$71.200 \pm 0.081 \text{ GeV}$	$74.454 \pm 0.076 \text{ GeV}$
$t\bar{t}dec - b\bar{b}4\ell$	$+365 \pm 110 \text{ MeV}$	$+161 \pm 102 \text{ MeV}$	$+75 \pm 97 \text{ MeV}$
$hvq - b\bar{b}4\ell$	$-563 \pm 110 \text{ MeV}$	$-456 \pm 103 \text{ MeV}$	$-323 \pm 97 \text{ MeV}$

Table 16. E_{b_j} peak position obtained with the $b\bar{b}4\ell$ generator showered with Pythia8.2, for three choices of the jet radius. The differences with the $t\bar{t}dec$ and the hvq generators are also shown.

a marked change in $E_{b_j}^{\max}$, that grows by 3.4 and 3.3 GeV when going from $R = 0.4$ to 0.5 and from 0.5 to 0.6 respectively, $t\bar{t}dec$ and hvq differ by $b\bar{b}4\ell$ by much smaller amounts. It is not clear whether such small differences could be discriminated experimentally.

According to eqs. (5.4) and (7.4), the uncertainties that affect the value of the extracted top mass are nearly twice the uncertainties on the b -jet energy. Considering the difference for $R = 0.5$ between hvq and $b\bar{b}4\ell$ in Tab. 16, we see that, by using hvq instead of $b\bar{b}4\ell$, the extracted top mass would be roughly 900 MeV larger. This should be compared with the corresponding difference of about 150 MeV, that is shown in Tab. 7, for the smeared m_{Wb_j} case.

As before, we have checked the sensitivity of our result to variations in the matching procedure in Pythia8.2, by studying the difference between **ScaleResonance** and **FSREmission** options. The differences turn out to be of the order of the statistical error.

7.2 Comparison with Herwig7.1

In this section, we study the dependence of our results on the shower MC program, comparing Herwig7.1 and Pythia8.2 predictions. We extract the differences in the $E_{b_j}^{\max}$ position for three values of the jet radius: $R = 0.4, 0.5$ and 0.6 . The results are summarized in Tab. 17, where we also show the results at the PS-only level, and in Fig. 16. From Tab. 17 we clearly see that the $b\bar{b}4\ell$ and the $t\bar{t}dec$ generators display larger discrepancies. For example, for the central value $R = 0.5$, we would get $\Delta E_{b_j}^{\max} \approx 2 \text{ GeV}$, that roughly corresponds to $\Delta m_t = -4 \text{ GeV}$. In the case of the hvq generator the difference is near 1 GeV, implying that the extracted mass using hvq +Herwig7.1 would be 2 GeV bigger than the one obtained with hvq +Pythia8.2.

We find that the differences between Herwig7.1 and Pythia8.2 increases for larger jet radii. Furthermore, by looking at Fig. 16, we notice that the $b\bar{b}4\ell$ generator displays

Pythia8.2 – Herwig7.1 [MeV]						
	$R = 0.4$		$R = 0.5$		$R = 0.6$	
	PS only	full	PS only	full	PS only	full
$b\bar{b}4\ell$	$+1297 \pm 120$	$+1631 \pm 122$	$+1666 \pm 117$	$+2150 \pm 114$	$+1802 \pm 114$	$+2356 \pm 113$
$t\bar{t}dec$	$+1786 \pm 91$	$+2039 \pm 91$	$+2179 \pm 88$	$+2332 \pm 88$	$+2121 \pm 89$	$+2437 \pm 87$
$h\nu q$	$+515 \pm 94$	$+762 \pm 93$	$+707 \pm 90$	$+1028 \pm 89$	$+779 \pm 87$	$+1188 \pm 86$

Table 17. Differences in the E_{b_j} peak position between the Pythia8.2 and the Herwig7.1 showers applied to the three generators for three choices of the jet radius. The results at the NLO+PS level (PS only) are also shown.

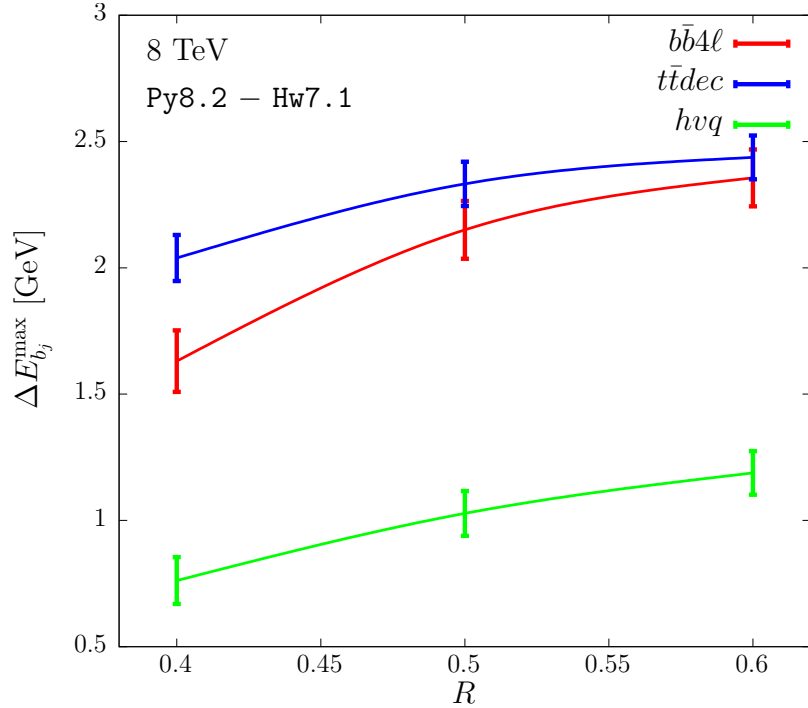


Figure 16. Differences of $E_{b_j}^{max}$ between the Pythia8.2 and the Herwig7.1 showers, for the three generators, as a function of the jet radius.

a different R dependence, as we have already observed from Tab. 16. Figure 16 indicates that $b\bar{b}4\ell$ and $t\bar{t}dec$ are in better agreement for larger values of the jet radius. This was also observed for the peak of the m_{Wb_j} smeared distribution (Tab. 7).

We notice that, as in the case of the reconstructed mass peak, the predominant contribution to the difference arises at the parton shower level.

As for the previous cases, we have examined the variations due to a different choice of the matching scheme in Herwig7.1, that we found to be below the 200 MeV level, and thus negligible in the present context.

8 Leptonic observables

In this section, we investigate the extraction of the top mass from the leptonic observables introduced in Ref. [28]. This method has been recently studied by the ATLAS collaboration in Ref. [65].

Following Ref. [28], we consider the subsequent five observables

$$\begin{aligned} O_1 &= p_T(\ell^+), & O_2 &= p_T(\ell^+\ell^-), & O_3 &= m(\ell^+\ell^-), \\ O_4 &= E(\ell^+\ell^-), & O_5 &= p_T(\ell^+) + p_T(\ell^-), \end{aligned}$$

i.e. the transverse momentum of the positive charged lepton, and the transverse momentum, the invariant mass, the energy and the scalar sum of the transverse momenta of the lepton pair. We compute the average value of the first three Mellin moments for each of the above mentioned observables, $\langle (O_i)^j \rangle$, with $i = 1, \dots, 5$ and $j = 1, 2, 3$. We assume that, if we do not vary too much the range of the top mass, we can write the linear relation

$$\langle (O_i)^j \rangle = O_c^{(ij)} + B^{(ij)} \left[(m_t)^j - (m_{t,c})^j \right]. \quad (8.1)$$

For ease of notation, we will refer to $O_c^{(ij)}$ and $B^{(ij)}$ as O_c and B in the following. Their determination will be discussed later.

We choose as reference sample the one generated with $b\bar{b}4\ell$ matched with **Pythia8.2**, using $m_{t,c} = 172.5$ GeV as input mass and the central choices for the PDF and scales. We indicate the values of the observables computed with this generator as $O^{b\bar{b}4\ell}$, and with O'_c the values of the observable computed either with an alternative generator or with different generator settings, but using as input parameter the same reference mass. The mass value that we would extracted from the events of the reference sample using the new generator is then given by

$$m'_t = \left[(m_{t,c})^j - \frac{O'_c - O^{b\bar{b}4\ell}}{B} \right]^{1/j}. \quad (8.2)$$

8.1 Comparison among NLO+PS generators

We begin by showing in Tabs. 18 and 19 the average values of the leptonic observables computed with our three NLO+PS generators interfaced with **Pythia8.2** and **Herwig7.1**. We show the central values, the differences with respect to $b\bar{b}4\ell$, and the upper and lower results induced by scale, PDF and α_s variations.

The scale and PDF variations are performed by reweighting. As a consequence of that, the associated error is much smaller than the statistical error on the cross section. In order to estimate it, we have divided our sample of events in ten sub-samples, computed the observables for each sub-sample, and carried out a straightforward statistical analysis on the ten sets of results. We found errors that never exceed the quoted value by more than 13%.

For the PDF variation, we have verified that differences due to variations in our reference PDF sets (see Sec. 6.1.2) are very similar among the different generators. On the other hand, a full error study using the **PDF4LHC15_nlo_30_pdfas** set was only performed

observable	gen	$\langle O_c \rangle$	% - $b\bar{b}4\ell$	(μ_F, μ_R)	PDF	α_s
$\langle p_T(\ell^+) \rangle$	$b\bar{b}4\ell$	56.653 ± 0.050 GeV	-	$^{+79}_{-86}$ MeV	-	± 26 (± 92) MeV
	$t\bar{t}dec$	56.804 ± 0.033 GeV	$+151 \pm 60$ MeV	$^{+84}_{-86}$ MeV	-	± 41 (± 23) MeV
	$h\nu q$	56.738 ± 0.032 GeV	$+85 \pm 59$ MeV	$^{+82}_{-86}$ MeV	± 130 MeV	± 49 (± 23) MeV
$\langle p_T(\ell^+ \ell^-) \rangle$	$b\bar{b}4\ell$	69.759 ± 0.059 GeV	-	$^{+710}_{-444}$ MeV	-	± 85 (± 110) MeV
	$t\bar{t}dec$	69.660 ± 0.040 GeV	-100 ± 71 MeV	$^{+538}_{-361}$ MeV	-	± 78 (± 28) MeV
	$h\nu q$	69.201 ± 0.038 GeV	-558 ± 71 MeV	$^{+553}_{-367}$ MeV	± 95 MeV	± 95 (± 27) MeV
$\langle m(\ell^+ \ell^-) \rangle$	$b\bar{b}4\ell$	108.685 ± 0.099 GeV	-	$^{+234}_{-341}$ MeV	-	± 57 (± 191) MeV
	$t\bar{t}dec$	108.812 ± 0.065 GeV	$+127 \pm 119$ MeV	$^{+244}_{-259}$ MeV	-	± 33 (± 46) MeV
	$h\nu q$	109.200 ± 0.064 GeV	$+515 \pm 118$ MeV	$^{+247}_{-265}$ MeV	± 395 MeV	± 68 (± 45) MeV
$\langle E(\ell^+ \ell^-) \rangle$	$b\bar{b}4\ell$	186.803 ± 0.163 GeV	-	$^{+342}_{-385}$ MeV	-	± 540 (± 305) MeV
	$t\bar{t}dec$	187.005 ± 0.107 GeV	$+201 \pm 195$ MeV	$^{+448}_{-434}$ MeV	-	± 474 (± 76) MeV
	$h\nu q$	186.809 ± 0.105 GeV	$+6 \pm 194$ MeV	$^{+441}_{-427}$ MeV	± 1068 MeV	± 559 (± 74) MeV
$\langle p_T(\ell^+) + p_T(\ell^-) \rangle$	$b\bar{b}4\ell$	113.322 ± 0.095 GeV	-	$^{+165}_{-184}$ MeV	-	± 93 (± 178) MeV
	$t\bar{t}dec$	113.598 ± 0.063 GeV	$+276 \pm 114$ MeV	$^{+165}_{-174}$ MeV	-	± 72 (± 44) MeV
	$h\nu q$	113.425 ± 0.062 GeV	$+104 \pm 113$ MeV	$^{+163}_{-177}$ MeV	± 259 MeV	± 101 (± 43) MeV

Table 18. The average values of each leptonic observable computed with $b\bar{b}4\ell$, $t\bar{t}dec$ and $h\nu q$, showered with **Pythia8.2**, for $m_t=172.5$ GeV, and their variations with respect to $b\bar{b}4\ell$ are shown in the first two columns. The differences with respect to their corresponding central values due to scale and PDF variations are also shown in columns three and four. Their α_s uncertainties, computed as described in Sec. 6.1.3 are displayed in column five. The statistical errors are also reported, except for the scale and PDF variations, where they have been estimated to be below 13% of the quoted values.

observable	gen	$\langle O_c \rangle$	% - $b\bar{b}4\ell$	(μ_F, μ_R)	PDF	α_s
$\langle p_T(\ell^+) \rangle$	$b\bar{b}4\ell$	56.104 ± 0.049 GeV	-	$^{+92}_{-106}$ MeV	-	± 20 (± 91) MeV
	$t\bar{t}dec$	56.199 ± 0.047 GeV	$+95 \pm 68$ MeV	$^{+90}_{-105}$ MeV	-	± 23 (± 23) MeV
	$h\nu q$	56.399 ± 0.032 GeV	$+295 \pm 59$ MeV	$^{+87}_{-100}$ MeV	± 222 MeV	± 45 (± 23) MeV
$\langle p_T(\ell^+ \ell^-) \rangle$	$b\bar{b}4\ell$	68.665 ± 0.059 GeV	-	$^{+587}_{-372}$ MeV	-	± 54 (± 108) MeV
	$t\bar{t}dec$	68.632 ± 0.051 GeV	-33 ± 78 MeV	$^{+452}_{-307}$ MeV	-	± 56 (± 28) MeV
	$h\nu q$	68.566 ± 0.038 GeV	-99 ± 70 MeV	$^{+466}_{-312}$ MeV	± 161 MeV	± 91 (± 27) MeV
$\langle m(\ell^+ \ell^-) \rangle$	$b\bar{b}4\ell$	108.497 ± 0.099 GeV	-	$^{+201}_{-265}$ MeV	-	± 24 (± 190) MeV
	$t\bar{t}dec$	108.076 ± 0.072 GeV	-422 ± 122 MeV	$^{+240}_{-250}$ MeV	-	± 2 (± 46) MeV
	$h\nu q$	109.056 ± 0.063 GeV	$+559 \pm 117$ MeV	$^{+247}_{-258}$ MeV	± 683 MeV	± 52 (± 45) MeV
$\langle E(\ell^+ \ell^-) \rangle$	$b\bar{b}4\ell$	185.540 ± 0.162 GeV	-	$^{+337}_{-380}$ MeV	-	± 504 (± 304) MeV
	$t\bar{t}dec$	185.315 ± 0.118 GeV	-225 ± 200 MeV	$^{+428}_{-416}$ MeV	-	± 426 (± 76) MeV
	$h\nu q$	186.125 ± 0.104 GeV	$+585 \pm 192$ MeV	$^{+420}_{-410}$ MeV	± 1842 MeV	± 520 (± 73) MeV
$\langle p_T(\ell^+) + p_T(\ell^-) \rangle$	$b\bar{b}4\ell$	112.280 ± 0.095 GeV	-	$^{+188}_{-218}$ MeV	-	± 52 (± 177) MeV
	$t\bar{t}dec$	112.455 ± 0.077 GeV	$+174 \pm 122$ MeV	$^{+177}_{-205}$ MeV	-	± 36 (± 45) MeV
	$h\nu q$	112.796 ± 0.061 GeV	$+516 \pm 112$ MeV	$^{+176}_{-204}$ MeV	± 444 MeV	± 97 (± 43) MeV

Table 19. As in Tab. 18 but for **Herwig7.1**.

	MEC – no MEC		
	$b\bar{b}4\ell$	$t\bar{t}dec$	$h\nu q$
$\langle p_T(\ell^+) \rangle$	$+117 \pm 74$ MeV	$+30 \pm 47$ MeV	$+342 \pm 46$ MeV
$\langle p_T(\ell^+\ell^-) \rangle$	$+167 \pm 89$ MeV	$+41 \pm 57$ MeV	$+544 \pm 55$ MeV
$\langle m(\ell^+\ell^-) \rangle$	$+171 \pm 149$ MeV	$+102 \pm 94$ MeV	$+631 \pm 91$ MeV
$\langle E(\ell^+\ell^-) \rangle$	$+372 \pm 243$ MeV	$+159 \pm 153$ MeV	$+1245 \pm 150$ MeV
$\langle p_T(\ell^+) + p_T(\ell^-) \rangle$	$+232 \pm 142$ MeV	$+85 \pm 89$ MeV	$+699 \pm 88$ MeV

Table 20. Impact of MEC in `Pythia8.2` on the leptonic observables for the different NLO+PS generators.

with the $h\nu q$ generator, and the associated errors exceed by far the variation band that we obtain with our reference sets. Thus, also in this case we quote the PDF variations only for $h\nu q$, implying that a very similar variation should also be present for the others. It is clear from the tables that the PDF uncertainties are dominant for several observables, and scale variations are also sizable.

The large variations in the α_s column are not always conclusive because of the large statistical errors (in parentheses), due to the fact that we cannot perform this variation by reweighting. However, unlike for the m_{Wb_j} case, here the PDF dependence is not small, and thus we cannot conclude that the α_s variation probes mainly the sensitivity to the intensity of radiation in decay, since when we vary α_s we change also the PDF set.

It is instead useful to look at the effect of MEC on the leptonic observables, displayed in Tab. 20. We observe that in the $b\bar{b}4\ell$ and $t\bar{t}dec$ case the effect of MEC is compatible with the statistical uncertainty. In the $h\nu q$ case we find instead sizable effects. This is expected, since large-angle radiation from the b quark, by subtracting energy to the whole Wb system, affects significantly also leptonic observables.

In Ref. [28] it was observed that the observables $p_T(\ell^+\ell^-)$ and $m(\ell^+\ell^-)$ had larger errors due to a stronger sensitivity to radiative corrections, and were more sensitive to spin-correlation effects. We see a confirmation of this observations in their larger errors due to scale variation, and in the fact that for $h\nu q$ their central value is shifted with respect to the $b\bar{b}4\ell$ and $t\bar{t}dec$ generators, that treat spin correlations in a better way.

In Tab. 21 we show the extracted values of the B coefficients for the first Mellin moment of each observable. The B values corresponding to the different generators are compatible within the statistical errors. We thus choose the values computed with the $h\nu q$ generator, that have the smallest error. According to eq. (8.2), we can translate a variation in an observable into a variation of the extracted mass, that for the first Mellin moment is simply obtained applying a $-1/B$ factor. The results are illustrated in Tab. 22. The errors shown have been obtained by summing in quadrature the statistical error and the scale and PDF uncertainties. We have not included the α_s variation in the error in order to avoid overcounting, since, in the present case, is likely to be largely dominated by the change in the associated PDF.

observable	generator	B
$\langle p_T(\ell^+) \rangle$	$b\bar{b}4\ell$	0.17 ± 0.04
	$t\bar{t}dec$	0.19 ± 0.02
	hvq	0.19 ± 0.02
$\langle p_T(\ell^+ \ell^-) \rangle$	$b\bar{b}4\ell$	0.30 ± 0.05
	$t\bar{t}dec$	0.30 ± 0.02
	hvq	0.29 ± 0.02
$\langle m(\ell^+ \ell^-) \rangle$	$b\bar{b}4\ell$	0.31 ± 0.08
	$t\bar{t}dec$	0.31 ± 0.03
	hvq	0.33 ± 0.03
$\langle E(\ell^+ \ell^-) \rangle$	$b\bar{b}4\ell$	0.55 ± 0.14
	$t\bar{t}dec$	0.56 ± 0.05
	hvq	0.56 ± 0.05
$\langle p_T(\ell^+) + p_T(\ell^-) \rangle$	$b\bar{b}4\ell$	0.38 ± 0.08
	$t\bar{t}dec$	0.39 ± 0.03
	hvq	0.39 ± 0.03

Table 21. Extracted B coefficients for the three different generators showered with `Pythia8.2`.

The overall errors on the last two lines of Tab. 22 are obtained with the same procedure adopted in Ref. [28] to account for correlations among the different observables. We do not see excessive differences among our three generators showered with the same Monte Carlo generator, while the differences between the `Pythia8.2` and `Herwig7.1` results are considerably large. This is also the case for the hvq generator, that has a much simpler interface to both `Pythia8.2` and `Herwig7.1`.

As we did for $m_{Wb_j}^{\max}$ and $E_{b_j}^{\max}$, also in the present case we have computed the leptonic observables without including hadronization effects, i.e. at parton-shower only level, in order to determine whether the differences between `Pythia8.2` and `Herwig7.1` are due to the shower or to the hadronization. Our findings are summarized in Tab. 23. Most of the differences already arises at the shower level. We also remark that, within the same SMC generator, they are not large, yielding differences in the extracted top mass of the same size as the statistical errors.

We observe in Tab. 22 that the inclusion of higher moments of the leptonic observables does not modify appreciably the results from the first moments. This is a consequence of the large error on the higher moments, and of the strong correlations among different moments.

The results in Tab. 22 are also summarized in Fig. 17, where the discrepancy between

observable	m_t extracted with Pythia8.2			m_t extracted with Herwig7.1		
	$b\bar{b}4\ell$	$t\bar{t}dec$	$h\nu q$	$b\bar{b}4\ell$	$t\bar{t}dec$	$h\nu q$
$\langle p_T(\ell^+) \rangle$	$172.500^{+0.845}_{-0.825}$	$171.719^{+0.821}_{-0.816}$	$172.060^{+0.822}_{-0.811}$	$175.340^{+1.298}_{-1.269}$	$174.847^{+1.293}_{-1.263}$	$173.817^{+1.270}_{-1.244}$
$\langle p_T(\ell^+ \ell^-) \rangle$	$172.500^{+1.601}_{-2.515}$	$172.848^{+1.315}_{-1.915}$	$174.451^{+1.334}_{-1.967}$	$176.328^{+1.433}_{-2.141}$	$176.442^{+1.227}_{-1.689}$	$176.675^{+1.235}_{-1.728}$
$\langle m(\ell^+ \ell^-) \rangle$	$172.500^{+1.605}_{-1.419}$	$172.116^{+1.441}_{-1.417}$	$170.945^{+1.450}_{-1.420}$	$173.068^{+2.233}_{-2.171}$	$174.342^{+2.208}_{-2.198}$	$171.379^{+2.214}_{-2.203}$
$\langle E(\ell^+ \ell^-) \rangle$	$172.500^{+2.061}_{-2.037}$	$172.138^{+2.081}_{-2.091}$	$172.490^{+2.076}_{-2.086}$	$174.771^{+3.393}_{-3.378}$	$175.176^{+3.401}_{-3.406}$	$173.720^{+3.397}_{-3.401}$
$\langle p_T(\ell^+) + p_T(\ell^-) \rangle$	$172.500^{+0.852}_{-0.827}$	$171.791^{+0.818}_{-0.806}$	$172.233^{+0.821}_{-0.802}$	$175.178^{+1.296}_{-1.265}$	$174.730^{+1.275}_{-1.246}$	$173.851^{+1.267}_{-1.239}$
$\langle p_T^2(\ell^+) \rangle$	$172.500^{+0.977}_{-0.960}$	$171.657^{+0.998}_{-1.011}$	$172.286^{+0.991}_{-1.007}$	$175.816^{+1.515}_{-1.502}$	$175.326^{+1.541}_{-1.524}$	$174.424^{+1.508}_{-1.497}$
$\langle p_T^2(\ell^+ \ell^-) \rangle$	$172.500^{+2.072}_{-3.375}$	$172.945^{+1.716}_{-2.585}$	$174.738^{+1.694}_{-2.577}$	$176.673^{+1.770}_{-2.725}$	$176.864^{+1.533}_{-2.170}$	$177.253^{+1.532}_{-2.199}$
$\langle m^2(\ell^+ \ell^-) \rangle$	$172.500^{+1.787}_{-1.643}$	$172.119^{+1.687}_{-1.680}$	$171.286^{+1.702}_{-1.695}$	$173.511^{+2.573}_{-2.569}$	$174.808^{+2.571}_{-2.595}$	$172.082^{+2.619}_{-2.644}$
$\langle E^2(\ell^+ \ell^-) \rangle$	$172.500^{+2.457}_{-2.462}$	$172.072^{+2.490}_{-2.534}$	$172.611^{+2.475}_{-2.518}$	$175.005^{+3.992}_{-4.067}$	$175.339^{+3.996}_{-4.093}$	$174.054^{+4.019}_{-4.117}$
$\langle (p_T(\ell^+) + p_T(\ell^-))^2 \rangle$	$172.500^{+1.076}_{-1.035}$	$171.642^{+1.036}_{-1.004}$	$172.198^{+1.043}_{-1.008}$	$175.489^{+1.608}_{-1.552}$	$174.982^{+1.563}_{-1.536}$	$174.145^{+1.566}_{-1.539}$
$\langle p_T^3(\ell^+) \rangle$	$172.500^{+1.269}_{-1.268}$	$171.558^{+1.273}_{-1.302}$	$172.626^{+1.262}_{-1.299}$	$176.472^{+1.801}_{-1.817}$	$175.877^{+1.861}_{-1.872}$	$175.212^{+1.798}_{-1.823}$
$\langle p_T^3(\ell^+ \ell^-) \rangle$	$172.500^{+2.912}_{-4.970}$	$173.092^{+2.435}_{-3.825}$	$175.316^{+2.333}_{-3.692}$	$177.424^{+2.355}_{-3.756}$	$177.691^{+2.075}_{-3.038}$	$178.410^{+2.046}_{-3.033}$
$\langle m^3(\ell^+ \ell^-) \rangle$	$172.500^{+2.172}_{-2.080}$	$172.416^{+2.089}_{-2.099}$	$171.834^{+2.124}_{-2.140}$	$173.978^{+3.170}_{-3.243}$	$175.662^{+3.127}_{-3.219}$	$172.980^{+3.237}_{-3.339}$
$\langle E^3(\ell^+ \ell^-) \rangle$	$172.500^{+2.958}_{-3.022}$	$172.003^{+2.998}_{-3.107}$	$172.843^{+2.963}_{-3.070}$	$175.349^{+4.701}_{-4.944}$	$175.515^{+4.704}_{-4.972}$	$174.576^{+4.744}_{-5.017}$
$\langle (p_T(\ell^+) + p_T(\ell^-))^3 \rangle$	$172.500^{+1.511}_{-1.428}$	$171.431^{+1.417}_{-1.374}$	$172.134^{+1.422}_{-1.373}$	$175.963^{+2.137}_{-2.022}$	$175.379^{+2.011}_{-1.995}$	$174.558^{+2.029}_{-2.012}$
all observables	$172.500^{+0.784}_{-0.766}$	$171.751^{+0.751}_{-0.751}$	$172.238^{+0.754}_{-0.748}$	$175.392^{+1.045}_{-1.138}$	$175.452^{+0.962}_{-1.104}$	$174.607^{+0.961}_{-1.097}$
1st moment	$172.500^{+0.794}_{-0.772}$	$171.755^{+0.764}_{-0.756}$	$172.247^{+0.766}_{-0.753}$	$175.440^{+1.102}_{-1.184}$	$175.445^{+1.011}_{-1.141}$	$174.756^{+1.010}_{-1.135}$

Table 22. Extracted mass in GeV for all the generators, showered with Pythia8.2 and Herwig7.1, corresponding to the different leptonic observables, using as reference sample the $b\bar{b}4\ell$ one generated with $m_t = 172.5$ GeV and showered with Pythia8.2. The quoted errors are obtained by summing in quadrature the scale, PDF and the statistical errors. The weighted average is also shown, for all the observables and considering only their first Mellin moment.

Pythia8.2 and Herwig7.1 and the mutual consistency of the different observables can be immediately appreciated.

As for the previous observables, we have studied the effect of changing the matching scheme, by switching between our two alternative matching schemes with Pythia8.2 and Herwig7.1, and by considering the settings of eq. (6.7) in Herwig7.1. In both cases we find results that are consistent within statistical errors.

9 Summary

In this work we have compared generators of increasing accuracy for the production and decay of $t\bar{t}$ pairs considering observables suitable for the measurement of the top mass. Rather than attempting to give a comprehensive assessments of the errors and uncertainties, we have focused upon those effects that can be tracked back to specific approximations and inaccuracies of the generators.

We have examined in particular the position of the peak in the spectrum of the reconstructed top mass, that we have introduced as an oversimplified representation of the observables used in direct top-mass measurements. This observable has proven to be the

		Py8.2 – Hw7.1 [MeV]	
observable	gen	full	PS only
$\langle p_{\text{T}}(\ell^+) \rangle$	$b\bar{b}4\ell$	$+549 \pm 70$	$+563 \pm 71$
	$t\bar{t}dec$	$+605 \pm 57$	$+609 \pm 48$
	$h\nu q$	$+340 \pm 45$	$+376 \pm 46$
$\langle p_{\text{T}}(\ell^+ \ell^-) \rangle$	$b\bar{b}4\ell$	$+1094 \pm 83$	$+1092 \pm 84$
	$t\bar{t}dec$	$+1027 \pm 65$	$+1020 \pm 59$
	$h\nu q$	$+636 \pm 54$	$+662 \pm 55$
$\langle m(\ell^+ \ell^-) \rangle$	$b\bar{b}4\ell$	$+188 \pm 140$	$+286 \pm 142$
	$t\bar{t}dec$	$+736 \pm 97$	$+814 \pm 98$
	$h\nu q$	$+144 \pm 90$	$+182 \pm 91$
$\langle E(\ell^+ \ell^-) \rangle$	$b\bar{b}4\ell$	$+1263 \pm 229$	$+1342 \pm 232$
	$t\bar{t}dec$	$+1690 \pm 160$	$+1712 \pm 159$
	$h\nu q$	$+684 \pm 148$	$+719 \pm 150$
$\langle p_{\text{T}}(\ell^+) + p_{\text{T}}(\ell^-) \rangle$	$b\bar{b}4\ell$	$+1041 \pm 134$	$+1091 \pm 136$
	$t\bar{t}dec$	$+1143 \pm 99$	$+1173 \pm 92$
	$h\nu q$	$+629 \pm 86$	$+690 \pm 88$

Table 23. Differences between the `Pythia8.2` and `Herwig7.1` results for the leptonic observables, at full hadron level and at parton-level only.

least sensitive to the generator choice and to its settings, and is in fact the one that yields smaller uncertainties.

A particularly important issue is whether, neglecting experimental uncertainties, i.e. assuming that we have knowledge of the final state at the particle level, the choice and settings of a generator leads to relevant intrinsic uncertainties in the extraction of the top mass. What we have in mind are potentially unknown perturbative and non-perturbative effects that may shift the position of the mass peak $m_{Wb_j}^{\text{max}}$. For example, if by comparing the $m_{Wb_j}^{\text{max}}$ value between a LO and NLO generator we find a sizable shift, we would have to conclude that also unknown higher-order effects may lead to a shift, thus giving an intrinsic uncertainty that we should estimate. On the other hand, if we find an insignificant variation, we may infer that the extracted mass is not very sensitive to higher-order effects. The same holds for scale and PDF variations, and for effects like interference of radiation from production and decay, that are included only in the most accurate generator. As far as these issues are concerned, we have seen that, within our `Pythia8.2` shower studies, no peak shifts above 30 MeV at the particle-truth level were observed. This also includes the

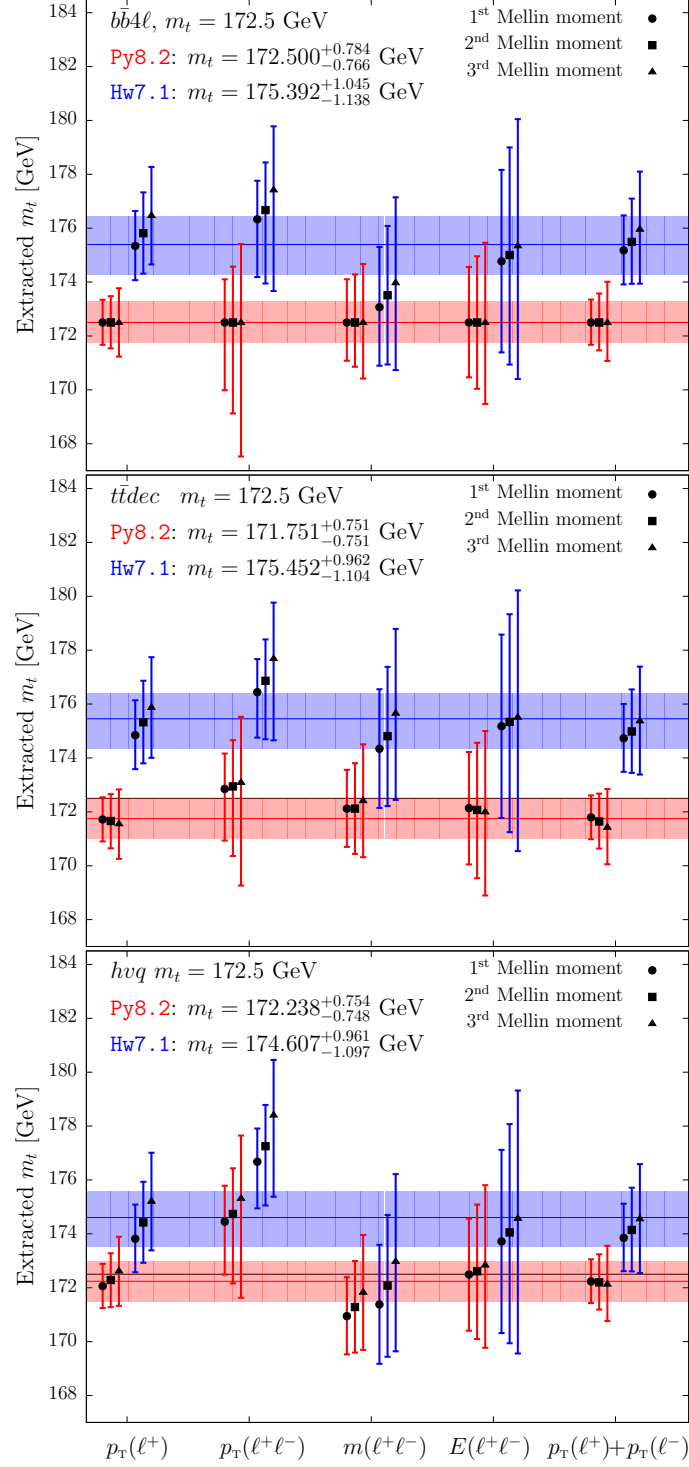


Figure 17. Extracted mass for the three generators matched with Pythia8.2 (red) and Herwig7.1 (blue) using the first three Mellin moments of the five leptonic observables. The horizontal band represents the weighted average of the results, and the black horizontal line corresponds to $m_t = 172.5$ GeV, which is the top mass value used in the $bb4l$ +Pythia8.2 reference sample.

comparison among the different NLO+PS generators. Even if we consider a setup such that radiation in top decay is treated only at leading order, i.e. the *h_vq* program interfaced to *Pythia8.2* with the MEC switched off, we find a shift in the peak of the non-smeared m_{Wb_j} distribution of only 61 MeV.

Larger shifts are seen for each NLO+PS generator if we change the shower program from *Pythia8.2* to *Herwig7.1*. The largest one, amounting to -235 MeV is observed in the *h_vq* case. In the $b\bar{b}4\ell$ and the $t\bar{t}dec$ cases the shift is of 66 MeV and 39 MeV respectively. In all cases the contribution is mostly due to the hadronization and underlying event, since the shift at the PS-only level is quite small. We have no good explanation for these differences among the various NLO+PS generators, since the hadronization stage should only depend upon the shower MC program. We also observe that, when using the internal POWHEG implementation of top decay, rather than the MEC, the -235 MeV shift drops essentially to few MeV, another feature that we do not fully understand.

Based upon the fact that the experimental resolution on the reconstructed top mass is roughly 15 GeV, we have also considered the $m_{Wb_j}^{\max}$ value extracted after a Gaussian smearing of the m_{Wb_j} distribution, with a Gaussian width of 15 GeV. In this context, when showering with *Pythia8.2*, we find modest differences in $m_{Wb_j}^{\max}$ among the different NLO+PS generators, with the *h_vq* result 147 MeV smaller, and the $t\bar{t}dec$ result 140 MeV larger than the $b\bar{b}4\ell$ one. A more significant deviation, equal to -1008 MeV, is found in the *h_vq* case if MEC are switched off in *Pythia8.2*. This feature is not surprising. Radiation from the b quark leads to a development of a tail below the peak in the m_{Wb_j} distribution, that however does not sensibly shift the peak position. After smearing, however, this tail causes a shift in the peak position. Since the tail is sensitive to large-angle radiation, relatively large differences are not surprising, when using only a leading-log description of b radiation rather than a POWHEG or MEC one.

Although the differences that we find are below the 200 MeV level, we believe that one should prefer the $b\bar{b}4\ell$ description, since it is the more accurate one. We also notice that, within $b\bar{b}4\ell$, scale-variation effects are estimated more realistically, and, together with the α_s variation that we have used to estimate uncertainties in radiation from the b quark, can be used to assess the uncertainties due to missing higher-order effects.

The most worrisome aspect of our findings for the smeared m_{Wb_j} distribution is the comparison between *Pythia8.2* and *Herwig7.1*. When comparing *Pythia8.2* and *Herwig7.1*, interfaced to either $b\bar{b}4\ell$ or $t\bar{t}dec$, we find differences near 1 GeV in the position of the peak. In the case of *h_vq*, we find a difference of 251 MeV, that increases to 607 MeV if the *Herwig7.1* internal POWHEG implementation of top decay (rather than the MEC) is used.

We have found that the large *Pythia8.2* – *Herwig7.1* differences are due to shower effects, i.e. that switching off the hadronization stage (including underlying events and MPI) does not make a significant change. At the moment we do not have further insights into the origin of these differences. We only remark that the shower models in *Pythia8.2* and *Herwig7.1* are quite different, the former implementing a dipole-type shower, while the latter uses an angular-ordered parton shower. On the positive side, we observe that, if the differences have a perturbative origin, they may be in principle reducible by improving the

theoretical model of the shower. Furthermore, we have also observed a different dependence of $m_{Wb_j}^{\max}$ upon the value of the jet R parameter in the `Pythia8.2` and `Herwig7.1` cases. This implies that both generators cannot fit the same data set, and that perhaps, by tuning them to yield the same R dependence, the differences in the $m_{Wb_j}^{\max}$ will also be reduced.

Another relatively simple mass-sensitive observable that we can examine with our three generators is the peak position ($E_{b_j}^{\max}$) of the b -jet energy (E_{b_j}) distribution, proposed in Ref. [27], where it is argued that this observable is relatively independent from production dynamics. We find, consistently with this claim, that the variations of $E_{b_j}^{\max}$ due to PDF and scale choices are of the order of few tens of MeV. On the other hand, we find clearly a strong dependence upon the modeling of the b jet. Focusing upon the `Pythia8.2` shower model, we find that the *h_vq* generator yields an $E_{b_j}^{\max}$ value that is smaller than the $b\bar{b}4\ell$ one by 456 MeV for $R = 0.5$. Furthermore, if the MEC are switched off, $E_{b_j}^{\max}$ decreases by another 1937 MeV. Comparing the `Pythia8.2` and `Herwig7.1` results, we also find very large differences, of the order of 2 GeV for $b\bar{b}4\ell$ and $t\bar{t}dec$, and 1 GeV for *h_vq*. Again, these shifts are dominated by the shower stage, and thus, in view of the insensitivity to the production mechanism, are likely to arise from final-state radiation off the b quark. In view of the fact that a variation in $E_{b_j}^{\max}$ implies a variation in the extracted mass that is twice as large, we see that, in order to get a competitive mass determination, the structure of the b jet should be better constrained.

The third class of observables that we have considered are the purely leptonic ones proposed in Ref. [28]. For these observables, we expect non-negligible dependence upon both the production and decay dynamics, and in fact we find non-negligible scale and PDF uncertainties, their size depending upon which observable is considered. This can be seen by inspecting Tabs. 18 and 19, and recalling that, from a variation in the lepton observable, we can obtain the corresponding m_t variation by multiplying it by the inverse of the B coefficients listed in Tab. 21. For example, for $\langle p_T(\ell^+) \rangle$ in Tab. 18, we get a variation due to PDF uncertainties of ± 130 MeV, that will correspond to an uncertainty in the extracted mass of the order of $\pm 130/0.19 = 684$ MeV.

We notice that changing the generator leads to sizable variations in our observables. In particular, the *h_vq* generator displays large deviations with respect to $b\bar{b}4\ell$ in $\langle p_T(\ell^+\ell^-) \rangle$ and $\langle m(\ell^+\ell^-) \rangle$. These two observables were argued to have stronger sensitivity to production dynamics details, like spin correlations, and in fact the *h_vq* generator is the least accurate from this point of view.

We expect that final-state radiation from the b quark may also affect leptonic observables via recoil effects. We see evidence of this aspect in the sensitivity of our result to the MEC implementation in `Pythia8.2` interfaced to the *h_vq* generator (see Tab. 20), where, for example, we see a variation of +342 MeV in $\langle p_T(\ell^+) \rangle$.

Also for the leptonic observables we find marked differences in the results obtained with `Pythia8.2` and `Herwig7.1` interfaced to each `POWHEG` generator. This is apparent from Fig. 17, where we observe a difference in the extracted mass that ranges from 2.4 to 3.7 GeV depending upon which `POWHEG` generator is used. We observe that also in this case, these differences arise already at the shower stage, and the hadronization and underlying-event contributions have only a minor impact.

10 Conclusions

In this paper we have studied a few observables relevant to the top-mass extraction using POWHEG generators of increasing accuracy. In particular we have considered the traditional $h\nu q$ POWHEG generator, that implements NLO correction in production, and also reaches essentially NLO accuracy in decay if used in conjunction with a parton-shower program that internally supports matrix-elements corrections, or POWHEG handling of top decay; the $t\bar{t}dec$ generator, that includes as further features NLO accuracy in top decay, NLO spin-correlation effects in the narrow-width approximation and non-resonant and off-shell effects at LO; and finally the $b\bar{b}4\ell$ generator that fully implements the process $pp \rightarrow b\bar{b}e^+\nu_e\mu^-\bar{\nu}_\mu$ taking appropriate care of the possible intermediate resonance histories. This last generator, that is our most advanced one, has limited our choice of observables, since, at the moment, it does not include W decays into hadrons.

We have introduced a reconstructed top-mass observable that represents a highly simplified model for all top-mass measurements that are generically referred to as “direct” or “standard” measurements, and are based upon a kinematic reconstruction of the top-decay products. We found that this observable, among those that we have considered, is the least affected by changes in parameters, POWHEG and shower generators.

We have considered the peak position in the b -jet energy distribution as an example of observables that should have little dependence upon the production dynamics, and verified that indeed this is the case. We have also seen, however, that it is very sensitive to jet modeling. On the other hand, the leptonic observables that we have considered have displayed sensitivity to both production and decay dynamics, at different levels.

Most of the effort undertaken in the present work has dealt with refining the interfaces between the POWHEG and the shower generators. In particular, the interface of the $t\bar{t}dec$ and $b\bar{b}4\ell$ POWHEG generators to Herwig7.1 has been developed for the first time in this work. Unlike all other shower interfaces in POWHEG, this is a non-trivial task, since the standard Les Houches interface for user processes [51] does not cover the case of coloured decaying resonances.

We have studied several sources of uncertainty of theoretical origin affecting the top-mass determination at hadron colliders. These do not cover all sources of uncertainties, but do cover effects that have never been considered before, and also suggest other directions to pursue in order to explore other uncertainties.

As far as the POWHEG uncertainties are concerned, we have not provided a sound estimate of errors associated with radiation effects. At the moment, the POWHEG framework does not allow to perform scale variation in the generation of radiation, so that we resorted to variations in α_s (and to the exclusion of MEC corrections in the $h\nu q$ case) in order to assess the sensitivity to the modeling of b -quark radiation. A better procedure for the study of these uncertainties is certainly desirable and not too difficult to achieve, and will be dealt with in future works.

Regarding the matching of the POWHEG generators to the parton shower, we have considered several alternatives in order to gain a reasonable confidence on our understanding of the related uncertainties. Yet, further investigation of these problems, in strict contact

with the developers of `Pythia8.2` and `Herwig7.1`, would be desirable, in order to make sure that no relevant issues have been overlooked.

Our study of the impact of shower and non-perturbative effects has been limited to a comparison between `Pythia8.2` and `Herwig7.1`. There, we have found particularly important differences, that with no doubt require further investigation. One question that remains open is whether by further tuning the shower programs to the same data set would reduce these differences.

It would be desirable to extend our investigation by considering variations in the parameters and in the setup of a single shower generator. In particular it would be interesting to examine the sensitivity to the colour-reconnection model, to the final-state radiation and initial-state radiation shower scales, to the shower scale cutoff, to the underlying-event parameters and to b -fragmentation parameters. Some of these studies are currently performed by the experimental collaborations in order to assess their systematic error. These tasks, however, can only be performed by an experimental collaboration within a given analysis framework, and are not the aim of the present work. It aims instead at tracking the origin of all uncertainties and differences associated with the variation of parameters and generator components, and understanding to what extent they can be reduced, in order to expose possible theoretical limitations to the ultimate accuracy achievable in top-mass measurements at hadron colliders.

Acknowledgments

We would like to thank Peter Richardson for important suggestions on the settings of `Herwig7.1` and on our `POWHEG-Herwig7.1` interfaces, and Stefan Prestel for help with the `Pythia8.2` code and for suggestions on the implementation of our `POWHEG-Pythia8.2` interface. We also like to thank Simon Plätzer and Stephen Webster for help and suggestions on our `Herwig7.1` input files, and for illustrating us aspects of the `Herwig7.1` code. Finally we thanks Roberto Franceschini, Alexander Mitov and Stefano Pozzorini for suggestions on the manuscript, and Mike Seymour, Peter Skands, Töbjoern Sjöstrand, Michelangelo Mangano, Andreas Papaefstathiou, and Andrzej Siodmok for useful discussions.

We acknowledge the CINECA and the Regione Lombardia award under the LISA initiative 2016-2018, for the availability of high performance computing resources and support. C.O. wishes to thank Maurizio Cremonesi for the help in running the code on the CINECA resources, under the project LISA PWHG-RES. The research of T.J. was supported by the Swiss National Science Foundation (SNF) under contracts BSCG10-157722 and CRSII2-160814.

A The treatment of remnants

In `POWHEG` it is possible to separate the real cross section, in a given singular region α , into two contributions

$$R^\alpha = R_s^\alpha + R_f^\alpha, \tag{A.1}$$

where R_f^α does not contain any singularities, while R_s^α is singular. Only R_s^α is exponentiated in the Sudakov form factor and used for the computation of \tilde{B} , while the leftover R_f^α , dubbed the remnant contribution, is finite upon phase space integration [36].

In all our three NLO generators it is possible to achieve this separation for initial-state radiation (ISR) emissions by setting the parameter `hdamp`¹² in the `powheg.input` file. Denoting with α_{ISR} the production region, $R_s^{\alpha_{\text{ISR}}}$ and $R_f^{\alpha_{\text{ISR}}}$ are defined as

$$R_s^{\alpha_{\text{ISR}}} = \frac{\text{hdamp}^2}{\text{hdamp}^2 + (p_T^{\alpha_{\text{ISR}}})^2} R^{\alpha_{\text{ISR}}}, \quad (\text{A.2})$$

$$R_f^{\alpha_{\text{ISR}}} = \frac{(p_T^{\alpha_{\text{ISR}}})^2}{\text{hdamp}^2 + (p_T^{\alpha_{\text{ISR}}})^2} R^{\alpha_{\text{ISR}}}, \quad (\text{A.3})$$

where $p_T^{\alpha_{\text{ISR}}}$ is the transverse momentum of the emitted parton relative to the beam axis. The `scalup` variable contained in the Les Houches event, that is used by the parton shower program to veto emissions harder than the POWHEG one, is set equal to $p_T^{\alpha_{\text{ISR}}}$.

Since remnant events are non-singular, the associated radiation has transverse momenta of the order of the partonic center-of-mass energy. We can thus define `scalup` as

$$\text{scalup} = \frac{\hat{s}}{2}. \quad (\text{A.4})$$

We have checked that, by using as `scalup` the default POWHEG scale (i.e. the transverse momentum of the radiated parton) the m_{Wb_j} and the $E_{b_j}^{\text{max}}$ values are very close to the ones we have presented in this paper. This is consistent with the expectation that these observables should be relatively insensitive to radiation in production, that in our case is always treated as ISR. The same holds for the leptonic observable $m(\ell^+\ell^-)$. For the remaining ones, a higher sensitivity to ISR effects is not excluded, and in fact the differences of the first Mellin moments reported in Tab. 18 with the corresponding ones obtained with the default `scalup` value, for the *hvg* generator showered with *Pythia8.2*, are given by

$$\begin{aligned} \delta\langle p_T(\ell^+) \rangle &= 125 \pm 46 \text{ MeV}, \\ \delta\langle p_T(\ell^+ + \ell^-) \rangle &= 298 \pm 54 \text{ MeV}, \\ \delta\langle E(\ell^+\ell^-) \rangle &= 214 \pm 149 \text{ MeV}, \\ \delta\langle p_T(\ell^+) + p_T(\ell^-) \rangle &= 219 \pm 87 \text{ MeV}. \end{aligned} \quad (\text{A.5})$$

In comparison with Tab. 18, we see that these variations are of the same order or smaller than those arising from scale and PDF uncertainties.

In the $b\bar{b}4\ell$ code, when ISR remnants are generated, no radiation in decay is produced.¹³ Thus, in this case, radiation off the resonances is fully handled by the parton shower, without the use of a veto algorithm to limit the p_T of the radiated partons.

The *ttdc* generator does instead implement radiation in decay also for remnants, and thus in this case vetoing is performed as for the standard events.

¹²We used an `hdamp` value equal to the input top-quark mass, i.e. the `qmass` parameter for the *hvg* generator, `tmass` for *b \bar{b} 4 ℓ* and *ttdc*.

¹³This behaviour may be changed in the future.

The absence of emissions from the t and \bar{t} resonances in remnant events for the $b\bar{b}4\ell$ generator, in contrast with the $t\bar{t}dec$ one, is probably the reason why the former generator displays a slightly larger sensitivity to matrix-element corrections (see Tabs. 4, 14 and 20).

To summarize:

- $h\nu q$: Emissions in decay are never vetoed. For remnant events the `scalup` value used to limit radiation in production is set to $\sqrt{\hat{s}}/2$.
- $t\bar{t}dec$: Emissions in decay are always vetoed. For remnant events the `scalup` value is set to $\sqrt{\hat{s}}/2$.
- $b\bar{b}4\ell$: Emissions in decay are always vetoed except if the event is a remnant, in which case they are never vetoed. For remnant events the `scalup` value is set to $\sqrt{\hat{s}}/2$.

B Fitting procedure

We always adopt the same fitting procedures in order to find the maximum of a distribution. Calling $Y(x)$ the histogram of our distribution, and $y(x, \{a\})$ our fitting functional form, where $\{a\}$ represent the fitting parameters, we proceed as follows:

- We find the bin with the highest value, and assign its center to the variable x_{\max} .
- We find all surrounding bins whose value is not less than $Y(x_{\max})/2$. We assign to the variable Δ the range covered by these bins divided by two.
- We minimize the χ^2 computed from the difference of the integral of $y(x, \{a\})$ in each bin, divided by the bin size, with respect to $Y(x)$, choosing as a range all bins that overlap with the segment $[x_{\max} - \Delta, x_{\max} + \Delta]$.
- From the fitted function we extract the maximum position and assign it to x_{\max} .
- If the reduced χ^2 of the fit is less than 2, we keep this result. If not, we replace $\Delta \rightarrow 0.95 \times \Delta$ and repeat the operation until this condition is met.

C PowhegHooks.h

In `Pythia8.2` the transverse-momentum definition used in the veto algorithm for radiation in production is different from the `POWHEG` one. In order to deal with this issue, the authors of `Pythia8.2` implemented a veto employing the `POWHEG` transverse momentum definition, by constructing a `UserHooks` subclass in the `PowhegHooks.h` file, which is currently part of the `Pythia8.2` distribution.

The `Pythia8.2` manual suggests to use the `PowhegHooks` class whenever showering a `POWHEG` style matched NLO+PS process. In order to implement the features of the `PowhegHooks` class in our generators, avoiding at the same time conflicts with the `PowhegHooksBB4L` one (that performs vetoing also for resonance decays), we added them to the `PowhegHooksBB4L` class, where they are activated by setting `POWHEG:veto = 1`.

PowhegHooks – no PowhegHooks [MeV]			
observable	$b\bar{b}4\ell$	$t\bar{t}dec$	$h\nu q$
$m_{Wb_j}^{\max}$ no smearing	35 ± 6	18 ± 5	17 ± 5
$m_{Wb_j}^{\max}$ smearing	77 ± 2	78 ± 2	71 ± 2
$E_{b_j}^{\max}$	4 ± 115	130 ± 87	157 ± 91
$\langle p_T(\ell^+) \rangle$	57 ± 70	74 ± 47	50 ± 46
$\langle p_T(\ell^+ \ell^-) \rangle$	166 ± 84	173 ± 56	150 ± 54
$\langle m(\ell^+ \ell^-) \rangle$	25 ± 140	16 ± 91	-18 ± 90
$\langle E(\ell^+ \ell^-) \rangle$	145 ± 230	143 ± 152	123 ± 149
$\langle p_T(\ell^+) + p_T(\ell^-) \rangle$	123 ± 135	144 ± 89	107 ± 87

Table 24. Differences between the predictions obtained using the POWHEG:veto = 1 and the POWHEG:veto = 0 settings for the three generators interfaced with Pythia8.2.

All the results presented in this paper were obtained using POWHEG:veto = 0. However, we have also investigated the sensitivity of our results to this setting, by showering all our samples with POWHEG:veto = 1. The differences with respect to the POWHEG:veto = 0 setting are listed in Tab. 24 for all the generators under study. The shifts obtained are not large and mostly compatible among the different generators.

D Truncated showers

We briefly remind the need for truncated showers in the specific example of a POWHEG implementation of top decay interfaced to an angular-ordered parton shower.

If top decay is treated without NLO corrections, the parton shower will generate radiation from the b quark with an unrestricted initial angle. The hardest radiation will take place along the shower after an arbitrary number of soft radiations at larger angles.

If POWHEG style NLO corrections are included, the hardest radiation, consisting in the emission of a gluon, will be generated first by POWHEG, and the parton shower will build angular-ordered jets starting from the b quark and the POWHEG gluon. The b quark will be assigned an initial angle for showering equal to θ_{bg} , the angle between the b and the POWHEG gluon. The soft radiation emitted by the b quark at angles larger than θ_{bg} will thus be missing. In order to remedy to this problem, it was proposed in Ref. [36] to let both the b quark and the gluon radiate with initial angle θ_{bg} and with a p_T veto set to the gluon relative transverse momentum, and to add a b quark p_T vetoed shower starting with the angle that would have been assigned if the gluon had not be radiated (i.e. an unrestricted angle), and stopping at the θ_{bg} angle.¹⁴

The veto technique introduced in Ref. [64], and activated in Herwig7.1 with the settings of eq. (6.7), performs a fully equivalent task. In fact, with these settings, the initial

¹⁴A simple example is also illustrated in Sec. 7.2 of Ref. [36].

angle for radiation from a gluon is taken as the maximum angle between the gluon and its two colour partners, that, in our case, leads to unrestricted radiation from the gluon, i.e. $\theta_{gg} \lesssim 1$. However, the color factor C_A associated with this radiation is reduced by a factor of two if $\theta_{gg} > \theta_{bg}$, while it is restored to C_A for smaller angles. Since $C_A/2 \approx C_F$ in the large N_c limit, we see that this is equivalent to the inclusion of a vetoed truncated shower from the b quark down to the angle θ_{bg} .

References

- [1] PARTICLE DATA GROUP collaboration, C. Patrignani et al., *Electroweak model and constraints on new physics, Review of Particle Physics*, *Chin. Phys.* **C40** (2016) 100001.
- [2] GFITTER GROUP collaboration, M. Baak, J. Cth, J. Haller, A. Hoecker, R. Kogler, K. Mnig et al., *The global electroweak fit at NNLO and prospects for the LHC and ILC*, *Eur. Phys. J.* **C74** (2014) 3046, [[1407.3792](#)].
- [3] ATLAS, CDF, CMS, D0 collaboration, *First combination of Tevatron and LHC measurements of the top-quark mass*, [arXiv:1403.4427](#).
- [4] ATLAS collaboration, M. Aaboud et al., *Measurement of the top quark mass in the $t\bar{t} \rightarrow$ dilepton channel from $\sqrt{s} = 8$ TeV ATLAS data*, *Phys. Lett.* **B761** (2016) 350–371, [[1606.02179](#)].
- [5] CMS collaboration, V. Khachatryan et al., *Measurement of the top quark mass using proton-proton data at $\sqrt{s} = 7$ and 8 TeV*, *Phys. Rev.* **D93** (2016) 072004, [[1509.04044](#)].
- [6] CMS collaboration, *Measurement of the top quark mass with lepton+jets final states in pp collisions at $\sqrt{s} = 13$ TeV*, Tech. Rep. CMS-PAS-TOP-17-007, CERN, Geneva, 2017.
- [7] ATLAS collaboration, *Measurement of the top quark mass in the $t\bar{t} \rightarrow$ lepton+jets channel from $\sqrt{s}=8$ TeV ATLAS data*, Tech. Rep. ATLAS-CONF-2017-071, CERN, Geneva, Sep, 2017.
- [8] B. Pearson, *Top quark mass in ATLAS*, in *10th International Workshop on Top Quark Physics (TOP2017) Braga, Portugal, September 17-22, 2017*, 2017. [1711.09763](#).
- [9] CMS collaboration, A. Castro, *Recent Top Quark Mass Measurements from CMS*, in *10th International Workshop on Top Quark Physics (TOP2017) Braga, Portugal, September 17-22, 2017*, 2017. [1712.01027](#).
- [10] G. Degrandi, S. Di Vita, J. Elias-Miro, J. R. Espinosa, G. F. Giudice, G. Isidori et al., *Higgs mass and vacuum stability in the Standard Model at NNLO*, *JHEP* **08** (2012) 098, [[1205.6497](#)].
- [11] D. Buttazzo, G. Degrandi, P. P. Giardinio, G. F. Giudice, F. Sala, A. Salvio et al., *Investigating the near-criticality of the Higgs boson*, *JHEP* **12** (2013) 089, [[1307.3536](#)].
- [12] A. Andreassen, W. Frost and M. D. Schwartz, *Scale Invariant Instantons and the Complete Lifetime of the Standard Model*, [1707.08124](#).
- [13] P. Nason, *The Top Mass in Hadronic Collisions*, [1712.02796](#).
- [14] A. H. Hoang, *The Top Mass: Interpretation and Theoretical Uncertainties*, in *Proceedings, 7th International Workshop on Top Quark Physics (TOP2014): Cannes, France, September 28-October 3, 2014*, 2014. [1412.3649](#).

- [15] I. I. Y. Bigi, M. A. Shifman, N. G. Uraltsev and A. I. Vainshtein, *The Pole mass of the heavy quark. Perturbation theory and beyond*, *Phys. Rev.* **D50** (1994) 2234–2246, [[hep-ph/9402360](#)].
- [16] M. Beneke and V. M. Braun, *Heavy quark effective theory beyond perturbation theory: Renormalons, the pole mass and the residual mass term*, *Nucl. Phys.* **B426** (1994) 301–343, [[hep-ph/9402364](#)].
- [17] M. Beneke, P. Marquard, P. Nason and M. Steinhauser, *On the ultimate uncertainty of the top quark pole mass*, *Phys. Lett.* **B775** (2017) 63–70, [[1605.03609](#)].
- [18] A. H. Hoang, C. Lepenik and M. Preisser, *On the Light Massive Flavor Dependence of the Large Order Asymptotic Behavior and the Ambiguity of the Pole Mass*, *JHEP* **09** (2017) 099, [[1706.08526](#)].
- [19] M. Beneke, Y. Kiyo, P. Marquard, A. Penin, J. Piclum and M. Steinhauser, *Next-to-Next-to-Next-to-Leading Order QCD Prediction for the Top Antitop S-Wave Pair Production Cross Section Near Threshold in e^+e^- Annihilation*, *Phys. Rev. Lett.* **115** (2015) 192001, [[1506.06864](#)].
- [20] F. Simon, *A First Look at the Impact of NNNLO Theory Uncertainties on Top Mass Measurements at the ILC*, in *Proceedings, International Workshop on Future Linear Colliders (LCWS15): Whistler, B.C., Canada, November 02-06, 2015*, 2016. [1603.04764](#).
- [21] S. Kawabata and H. Yokoya, *Top-quark mass from the diphoton mass spectrum*, *Eur. Phys. J.* **C77** (2017) 323, [[1607.00990](#)].
- [22] S. Alioli, P. Fernandez, J. Fuster, A. Irlles, S.-O. Moch, P. Uwer et al., *A new observable to measure the top-quark mass at hadron colliders*, *Eur. Phys. J.* **C73** (2013) 2438, [[1303.6415](#)].
- [23] S. Kawabata, Y. Shimizu, Y. Sumino and H. Yokoya, *Weight function method for precise determination of top quark mass at Large Hadron Collider*, *Phys. Lett.* **B741** (2015) 232–238, [[1405.2395](#)].
- [24] J. Gao, C. S. Li and H. X. Zhu, *Top Quark Decay at Next-to-Next-to Leading Order in QCD*, *Phys. Rev. Lett.* **110** (2013) 042001, [[1210.2808](#)].
- [25] M. Brucherseifer, F. Caola and K. Melnikov, *$\mathcal{O}(\alpha_s^2)$ corrections to fully-differential top quark decays*, *JHEP* **04** (2013) 059, [[1301.7133](#)].
- [26] A. H. Hoang, S. Mantry, A. Pathak and I. W. Stewart, *Extracting a Short Distance Top Mass with Light Grooming*, [1708.02586](#).
- [27] K. Agashe, R. Franceschini, D. Kim and M. Schulze, *Top quark mass determination from the energy peaks of b-jets and B-hadrons at NLO QCD*, *Eur. Phys. J.* **C76** (2016) 636, [[1603.03445](#)].
- [28] S. Frixione and A. Mitov, *Determination of the top quark mass from leptonic observables*, *JHEP* **09** (2014) 012, [[1407.2763](#)].
- [29] CMS collaboration, A. M. Sirunyan et al., *Measurement of the top quark mass in the dileptonic $t\bar{t}$ decay channel using the mass observables $M_{b\ell}$, M_{T2} , and $M_{b\ell\nu}$ in pp collisions at $\sqrt{s} = 8$ TeV*, *Phys. Rev.* **D96** (2017) 032002, [[1704.06142](#)].
- [30] C. G. Lester and D. J. Summers, *Measuring masses of semiinvisibly decaying particles pair produced at hadron colliders*, *Phys. Lett.* **B463** (1999) 99–103, [[hep-ph/9906349](#)].

- [31] A. J. Barr, B. Gripaios and C. G. Lester, *Transverse masses and kinematic constraints: from the boundary to the crease*, *JHEP* **11** (2009) 096, [[0908.3779](#)].
- [32] CMS collaboration, *Determination of the normalised invariant mass distribution of $t\bar{t}$ +jet and extraction of the top quark mass*, Tech. Rep. CMS-PAS-TOP-13-006, CERN, Geneva, 2016.
- [33] CMS collaboration, *Measurement of the top-quark mass from the b jet energy spectrum*, Tech. Rep. CMS-PAS-TOP-15-002, CERN, Geneva, 2015.
- [34] ATLAS collaboration, G. Aad et al., *Determination of the top-quark pole mass using $t\bar{t}$ + 1-jet events collected with the ATLAS experiment in 7 TeV pp collisions*, *JHEP* **10** (2015) 121, [[1507.01769](#)].
- [35] ATLAS collaboration, M. Aaboud et al., *Measurement of lepton differential distributions and the top quark mass in $t\bar{t}$ production in pp collisions at $\sqrt{s} = 8$ TeV with the ATLAS detector*, [1709.09407](#).
- [36] P. Nason, *A New method for combining NLO QCD with shower Monte Carlo algorithms*, *JHEP* **11** (2004) 040, [[hep-ph/0409146](#)].
- [37] S. Frixione, P. Nason and C. Oleari, *Matching NLO QCD computations with Parton Shower simulations: the POWHEG method*, *JHEP* **11** (2007) 070, [[0709.2092](#)].
- [38] S. Alioli, P. Nason, C. Oleari and E. Re, *A general framework for implementing NLO calculations in shower Monte Carlo programs: the POWHEG BOX*, *JHEP* **06** (2010) 043, [[1002.2581](#)].
- [39] J. M. Campbell, R. K. Ellis, P. Nason and E. Re, *Top-pair production and decay at NLO matched with parton showers*, *JHEP* **04** (2015) 114, [[1412.1828](#)].
- [40] T. Ježo, J. M. Lindert, P. Nason, C. Oleari and S. Pozzorini, *An NLO+PS generator for $t\bar{t}$ and Wt production and decay including non-resonant and interference effects*, *Eur. Phys. J.* **C76** (2016) 691, [[1607.04538](#)].
- [41] S. Frixione, P. Nason and G. Ridolfi, *A Positive-weight next-to-leading-order Monte Carlo for heavy flavour hadroproduction*, *JHEP* **09** (2007) 126, [[0707.3088](#)].
- [42] T. Sjöstrand, S. Ask, J. R. Christiansen, R. Corke, N. Desai, P. Ilten et al., *An Introduction to PYTHIA 8.2*, *Comput. Phys. Commun.* **191** (2015) 159–177, [[1410.3012](#)].
- [43] M. Bahr et al., *Herwig++ Physics and Manual*, *Eur. Phys. J.* **C58** (2008) 639–707, [[0803.0883](#)].
- [44] J. Bellm et al., *Herwig 7.0/Herwig++ 3.0 release note*, *Eur. Phys. J.* **C76** (2016) 196, [[1512.01178](#)].
- [45] D. Wicke and P. Z. Skands, *Non-perturbative QCD Effects and the Top Mass at the Tevatron*, *Nuovo Cim.* **B123** (2008) S1, [[0807.3248](#)].
- [46] T. Sjöstrand, *Colour reconnection and its effects on precise measurements at the LHC*, 2013, [1310.8073](#).
- [47] A. Andreassen and M. D. Schwartz, *Reducing the Top Quark Mass Uncertainty with Jet Grooming*, *JHEP* **10** (2017) 151, [[1705.07135](#)].
- [48] G. Heinrich, A. Maier, R. Nisius, J. Schlenk, M. Schulze, L. Scyboz et al., *NLO and off-shell effects in top quark mass determinations*, [1709.08615](#).

- [49] G. Bevilacqua, H. B. Hartanto, M. Kraus, M. Schulze and M. Worek, *Top quark mass studies with $t\bar{t}j$ at the LHC*, [1710.07515](#).
- [50] S. Frixione, E. Laenen, P. Motylinski and B. R. Webber, *Angular correlations of lepton pairs from vector boson and top quark decays in Monte Carlo simulations*, *JHEP* **04** (2007) 081, [[hep-ph/0702198](#)].
- [51] E. Boos et al., *Generic user process interface for event generators*, in *Physics at TeV colliders. Proceedings, Euro Summer School, Les Houches, France, May 21-June 1, 2001*, 2001. [hep-ph/0109068](#).
- [52] T. Ježo and P. Nason, *On the Treatment of Resonances in Next-to-Leading Order Calculations Matched to a Parton Shower*, *JHEP* **12** (2015) 065, [[1509.09071](#)].
- [53] R. Frederix, S. Frixione, A. S. Papanastasiou, S. Prestel and P. Torrielli, *Off-shell single-top production at NLO matched to parton showers*, *JHEP* **06** (2016) 027, [[1603.01178](#)].
- [54] F. Cascioli, P. Maierhofer and S. Pozzorini, *Scattering Amplitudes with Open Loops*, *Phys. Rev. Lett.* **108** (2012) 111601, [[1111.5206](#)].
- [55] <http://home.thep.le.se/Pythia/pythia82html/UserHooks.html>.
- [56] A. D. Martin, W. J. Stirling, R. S. Thorne and G. Watt, *Parton distributions for the LHC*, *Eur. Phys. J. C* **63** (2009) 189–285, [[0901.0002](#)].
- [57] M. Cacciari, G. P. Salam and G. Soyez, *FastJet User Manual*, *Eur. Phys. J. C* **72** (2012) 1896, [[1111.6097](#)].
- [58] M. Cacciari, G. P. Salam and G. Soyez, *The Anti- $k(t)$ jet clustering algorithm*, *JHEP* **04** (2008) 063, [[0802.1189](#)].
- [59] J. Butterworth et al., *PDF4LHC recommendations for LHC Run II*, *J. Phys. G* **43** (2016) 023001, [[1510.03865](#)].
- [60] S. Dulat, T.-J. Hou, J. Gao, M. Guzzi, J. Huston, P. Nadolsky et al., *New parton distribution functions from a global analysis of quantum chromodynamics*, *Phys. Rev. D* **93** (2016) 033006, [[1506.07443](#)].
- [61] L. A. Harland-Lang, A. D. Martin, P. Motylinski and R. S. Thorne, *Parton distributions in the LHC era: MMHT 2014 PDFs*, *Eur. Phys. J. C* **75** (2015) 204, [[1412.3989](#)].
- [62] NNPDF collaboration, R. D. Ball et al., *Parton distributions for the LHC Run II*, *JHEP* **04** (2015) 040, [[1410.8849](#)].
- [63] G. Corcella, R. Franceschini and D. Kim, *Fragmentation Uncertainties in Hadronic Observables for Top-quark Mass Measurements*, [1712.05801](#).
- [64] A. Schofield and M. H. Seymour, *Jet vetoing and Herwig++*, *JHEP* **01** (2012) 078, [[1103.4811](#)].
- [65] ATLAS collaboration, *Measurement of lepton differential distributions and the top quark mass in $t\bar{t}$ production in pp collisions at $\sqrt{s} = 8$ TeV with the ATLAS detector*, Tech. Rep. ATLAS-CONF-2017-044, CERN, Geneva, Jul, 2017.